PERGAMON

Planetary and Space Science 49 (2001) 1445–1465

Planetary and Space Science

www.elsevier.com/locate/planspasci

The MESSENGER mission to Mercury: scientific objectives and implementation

Sean C. Solomon[a,*], Ralph L. McNutt Jr.[b], Robert E. Gold[b], Mario H. Acuña[c], Daniel N. Baker[d], William V. Boynton[e], Clark R. Chapman[f], Andrew F. Cheng[b], George Gloeckler[g,h], James W. Head III[i], Stamatios M. Krimigis[b], William E. McClintock[d], Scott L. Murchie[b], Stanton J. Peale[j], Roger J. Phillips[k], Mark S. Robinson[l], James A. Slavin[c], David E. Smith[c], Robert G. Strom[e], Jacob I. Trombka[c], Maria T. Zuber[m]

[a] *Department of Terrestrial Magnetism, Carnegie Institution of Washington, Washington, DC 20015, USA*
[b] *The Johns Hopkins University Applied Physics Laboratory, Laurel, MD 20723, USA*
[c] *NASA Goddard Space Flight Center, Greenbelt, MD 20771, USA*
[d] *Laboratory for Atmospheric and Space Physics, University of Colorado, Boulder, CO 80303, USA*
[e] *Lunar and Planetary Laboratory, University of Arizona, Tucson, AZ 85721, USA*
[f] *Southwest Research Institute, Boulder, CO 80302, USA*
[g] *Department of Physics, University of Maryland, College Park, MD 20742, USA*
[h] *Department of Atmospheric, Oceanic, and Space Sciences, University of Michigan, Ann Arbor, MI 48109, USA*
[i] *Department of Geological Sciences, Brown University, Providence, RI 02912, USA*
[j] *Department of Physics, University of California, Santa Barbara, CA 93106, USA*
[k] *Department of Earth and Planetary Sciences, Washington University, St. Louis, MO 63130, USA*
[l] *Department of Geological Sciences, Northwestern University, Evanston, IL 60208, USA*
[m] *Department of Earth, Atmospheric, and Planetary Sciences, Massachusetts Institute of Technology, Cambridge, MA 02139, USA*

Received 1 November 2000; accepted 12 January 2001

Abstract

Mercury holds answers to several critical questions regarding the formation and evolution of the terrestrial planets. These questions include the origin of Mercury's anomalously high ratio of metal to silicate and its implications for planetary accretion processes, the nature of Mercury's geological evolution and interior cooling history, the mechanism of global magnetic field generation, the state of Mercury's core, and the processes controlling volatile species in Mercury's polar deposits, exosphere, and magnetosphere. The MErcury Surface, Space ENvironment, GEochemistry, and Ranging (MESSENGER) mission has been designed to fly by and orbit Mercury to address all of these key questions. After launch by a Delta 2925H-9.5, two flybys of Venus, and two flybys of Mercury, orbit insertion is accomplished at the third Mercury encounter. The instrument payload includes a dual imaging system for wide and narrow fields-of-view, monochrome and color imaging, and stereo; X-ray and combined gamma-ray and neutron spectrometers for surface chemical mapping; a magnetometer; a laser altimeter; a combined ultraviolet–visible and visible-near-infrared spectrometer to survey both exospheric species and surface mineralogy; and an energetic particle and plasma spectrometer to sample charged species in the magnetosphere. During the flybys of Mercury, regions unexplored by Mariner 10 will be seen for the first time, and new data will be gathered on Mercury's exosphere, magnetosphere, and surface composition. During the orbital phase of the mission, one Earth year in duration, MESSENGER will complete global mapping and the detailed characterization of the exosphere, magnetosphere, surface, and interior.

1. Introduction

Mercury is the least studied planet save Pluto. Much of what is known (Vilas et al., 1988) comes from the three flybys of Mercury by Mariner 10 in 1974 and 1975. Mariner 10 imaged about 45% of the surface at an average resolution of about 1 km and less than 1% of the surface at better than 500-m resolution (Murray, 1975). Further, Mariner 10 discovered the planet's internal magnetic field (Ness et al., 1974, 1975); measured the ultraviolet signatures of H, He, and O in Mercury's atmosphere (Broadfoot et al.,

* Corresponding author. Tel.: +1-202-478-8850; fax: +1-202-478-8821.
E-mail address: scs@dtm.ciw.edu (S.C. Solomon).

0032-0633/01/$ - see front matter
PII: S0032-0633(01)00085-X

1974, 1976); documented the time-variable nature of Mercury's magnetosphere (Ogilvie et al., 1974; Simpson et al., 1974); and determined some of the physical characteristics of Mercury's surface materials (Chase et al., 1974). Important subsequent ground-based discoveries include the Na, K, and Ca components of the atmosphere (Potter and Morgan, 1985, 1986; Bida et al., 2000) and the radar-reflective polar deposits (Slade et al., 1992; Harmon and Slade, 1992).

A substantially improved knowledge of the planet Mercury is critical to our understanding of how terrestrial planets formed and evolved. Determining the surface composition of Mercury, a body with a ratio of metal to silicate higher than any other planet or satellite, will provide a unique window on the processes by which planetesimals in the primitive solar nebula accreted to form planets. Documenting the global geological history will elucidate the role of planet size as a governor of magmatic and tectonic history for a terrestrial planet. Characterizing the nature of the magnetic field of Mercury and the size and state of Mercury's core will allow us to generalize our understanding of the energetics and lifetimes of magnetic dynamos, as well as core and mantle thermal histories, in solid planets and satellites. Determining the nature of volatile species in Mercury's polar deposits, atmosphere, and magnetosphere will provide critical insight into volatile inventories, sources, and sinks in the inner solar system.

MESSENGER is a MErcury Surface, Space ENvironment, GEochemistry, and Ranging mission designed to achieve these aims. As part of the Discovery Program of the National Aeronautics and Space Administration (NASA), the MESSENGER spacecraft will orbit Mercury for one Earth year after completing two flybys of that planet following two flybys of Venus. The necessary flybys return significant new data early in the mission, while the orbital phase, guided by the flyby data, enables a focused scientific investigation of this least-studied terrestrial planet. Answers to key questions about Mercury's high density, crustal composition and structure, volcanic history, core structure, magnetic field generation, polar deposits, atmosphere, overall volatile inventory, and magnetosphere are provided by an optimized set of miniaturized space instruments. In this paper, we first describe the rationale for and scientific objectives of the MESSENGER mission. We then summarize the mission implementation plan designed to satisfy those objectives. In companion papers, we present details of the MESSENGER scientific payload (Gold et al., 2001) and the MESSENGER spacecraft and mission design (Santo et al., 2001).

2. Scientific rationale for MESSENGER

The MESSENGER mission has been designed to address six key scientific questions. The answers to these questions bear not only on the nature of the planet Mercury but also more generally on the origin and comparative evolution of all of the terrestrial planets.

2.1. What planetary formational processes led to the high metal/silicate ratio in Mercury?

Perhaps the question of greatest importance for our understanding of terrestrial planet formation is the origin of Mercury's high uncompressed density (about $5.3\,Mg/m^3$). Interior structure models in which a dominantly iron core has fully differentiated from the overlying silicate mantle indicate that the core radius is approximately 75% of the planetary radius and the fractional core mass about 65% (Siegfried and Solomon, 1974). This metallic mass fraction is more than twice that of the Earth, Venus, or Mars. At one time, the high density was attributed (Lewis, 1972) to the slightly higher condensation temperature of iron compared with magnesian silicates in the cooling solar nebula, such that at Mercury's distance from the protosun the ratio of solid metal to silicate was much higher than in the formation zones of the other terrestrial planets. Subsequent calculations of dynamically plausible accretion scenarios, however, have shown that the terrestrial planets probably formed from material originally occupying a wide range in solar distance (Wetherill, 1988, 1994). In particular, Mercury-size bodies can experience wide migrations of their semimajor axes during their growth (Wetherill, 1988). Given such scenarios, equilibrium condensation models cannot account for the high metal/silicate ratio in Mercury (Goettel and Barshay, 1978; Lewis, 1988).

There are currently three classes of explanations for the high metal fraction of Mercury. One class invokes differences in the response of iron and silicate particles to aerodynamic drag by solar nebular gas to achieve fractionation at the onset of planetesimal accretion (Weidenschilling, 1978). The second and third class of explanations invoke processes late in the planetary accretion process, after the Mercury protoplanet had differentiated silicate mantle from metal core. In one, the high metal content of Mercury is attributed to preferential vaporization of silicates by solar radiation early in the Sun's evolution (Cameron, 1985; Fegley and Cameron, 1987). In the other, selective removal of silicate occurred as a result of a giant impact (Wetherill, 1988; Benz et al., 1988).

These three hypotheses lead to different predictions for the bulk chemistry of the silicate fraction of Mercury (Lewis, 1988). Under the impact hypothesis, the residual silicate material on Mercury would be dominantly of mantle composition. The FeO content would reflect the oxidation state of the material from which the protoplanet accreted, but the loss of much of the original crust would deplete Ca, Al, and alkali metals without enriching refractory elements. The vaporization model, in contrast, predicts strong enrichment of refractory elements and depletion of alkalis and FeO (Fegley and Cameron, 1987). Under both of these models, the present

crust should represent primarily the integrated volume of magma produced by partial melting of the relic mantle. Under the aerodynamic sorting model (Weidenschilling, 1978), the core and silicate portions of Mercury may be adequately described by condensation models, suitably weighted by solar distance, except that the ratio of metal to silicate is much larger (Lewis, 1988). This model permits a thick primordial crust, i.e., one produced by crystal-liquid fractionation of a silicate magma ocean. With any of the three models, late infall of cometary and asteroidal material may have influenced surface and near-surface chemistry.

Determining the bulk chemistry of the silicate portion of Mercury thus offers the unique opportunity to learn which of the mechanisms operating during the formation of the inner solar system had the greatest influence on the bulk composition of the inner planets. Present information on the chemistry and mineralogy of the surface of Mercury, however, is far too limited to distinguish clearly among the competing hypotheses. Ground-based reflectance spectra at visible, infrared, and millimeter wavelengths suggest generally low FeO and high alkali feldspar contents (Vilas, 1988; Sprague et al., 1994, 1997; Jeanloz et al., 1995; Blewett et al., 1997). The observations of K and Na in Mercury's tenuous atmosphere favor significant alkali contents, although whether the source for these species is a surficial veneer of meteoritic material or deeper regions of the Mercury crust is not known (Hunten et al., 1988). An important adjunct to direct determination of the chemistry of surface materials, including those ejected by large impacts from some depth, would be an estimate of the thickness of Mercury's crust. The thickness can be estimated by a combined analysis of gravity and topography measurements if such data are sensitive to variations on horizontal scales of several hundred kilometers and greater (Zuber et al., 1994; Simons et al., 1997).

2.2. What is the geological history of Mercury?

Because of Mercury's size, intermediate between the Moon and Mars, as well as its high metal/silicate ratio, documenting the geological history of Mercury is crucial to understanding how terrestrial planet evolution depends on planet size and initial conditions. A generalized geological history of Mercury has been developed from Mariner 10 images (e.g., Strom, 1979, 1997; Spudis and Guest, 1988), but the limited coverage and resolution of those images render that history uncertain.

Most of the 45% of Mercury imaged by Mariner 10 can be divided into four major terrains. Heavily cratered regions (Fig. 1) have an impact crater density suggesting that this terrain records the period of heavy bombardment that ended about 3.8 billion years ago on the Moon. Intercrater plains (Fig. 2), the most extensive terrain type, were emplaced over a range of ages during the period of heavy bombardment. Intercrater plains may be either of volcanic or impact origin,

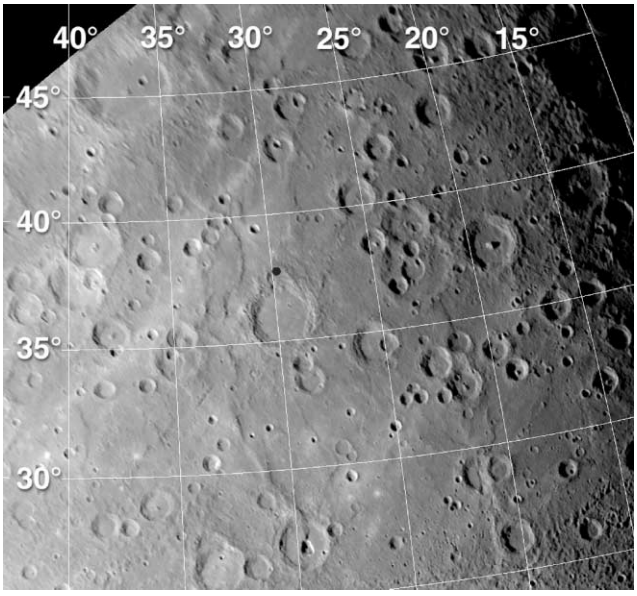

Fig. 1. Much of the surface of Mercury is heavily cratered, as in this mosaic of images acquired during the first Mariner 10 flyby of Mercury (Robinson et al., 1999). Portions of inter-crater regions have been resurfaced by plains of varying age.

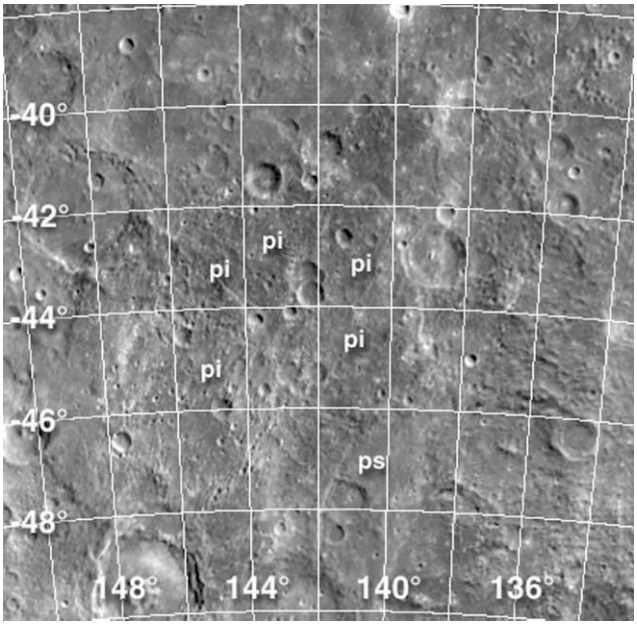

Fig. 2. An example of intercrater plains. Whether such plains are made up of ejecta deposits from basin-forming impacts or are primarily volcanic in origin remains unsettled (Spudis and Guest, 1988). The region shown is a mosaic of images acquired during the second Mariner 10 flyby of Mercury (Robinson et al., 1999). Areas of intercrater plains are indicated by the notation pi, and a small area of smooth plains is denoted by ps (Spudis and Prosser, 1984).

but there are no diagnostic morphological features to distinguish between these two possibilities visible at Mariner 10 resolution. Hilly and lineated terrain (Fig. 3) occurs

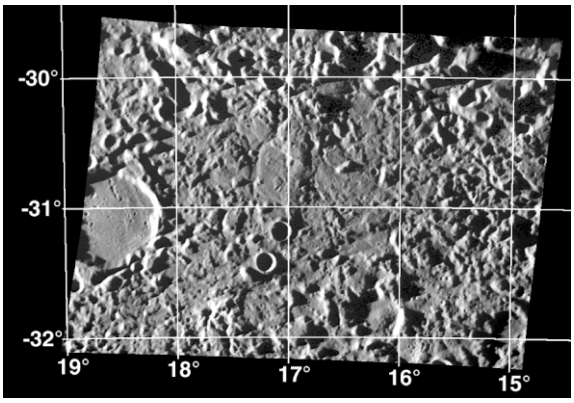

Fig. 3. An example of hilly and lineated terrain (Mariner 10 image 27463, 163 m/pixel). The region shown is antipodal to the Caloris Basin and is thought to have developed its distinctive morphology by the focusing of shock waves generated by the Caloris impact (Gault et al., 1975).

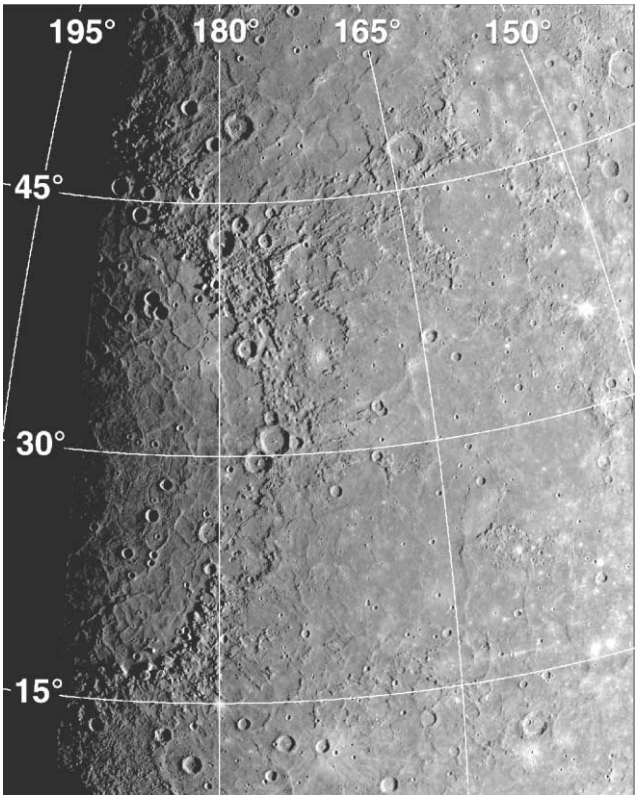

Fig. 4. The eastern half of the 1340-km-diameter Caloris Basin. This image is a portion of the controlled Mariner 10 mosaic of Robinson et al. (1999); orthographic projection, 1 km/pixel.

antipodal to the Caloris basin, at 1300-km diameter the largest known impact structure on Mercury (Fig. 4), and is thought to have originated at the time of the Caloris impact by the focusing of impact-generated shock waves (Gault et al., 1975). Smooth plains (Fig. 5), the youngest terrain type, cover 40% of the area imaged by Mariner 10 and are mostly associated with large impact basins. In a stratigraphic posi-

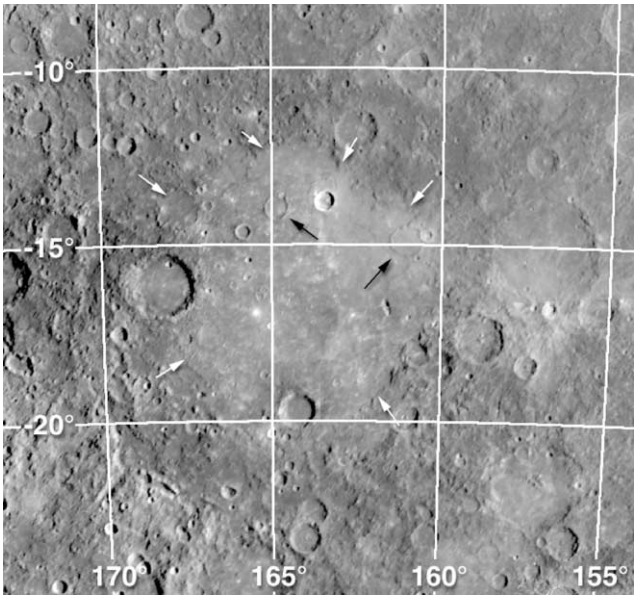

Fig. 5. Smooth plains fill the center of the 510-km-diameter Tolstoj Basin (unit boundaries shown as white arrows) and partially fill smaller craters (black arrows) on the basin floor. These superposition relationships indicate that this region of smooth plains cannot be impact melt generated at the time of formation of the Tolstoj Basin. The image is a portion of a hemispheric mosaic with a resolution of 1 km/pixel.

tion similar to that of the lunar maria, they are thought to be volcanic deposits on the basis of their relative age, visible color properties (Hapke et al., 1980; Rava and Hapke, 1987; Robinson and Lucey, 1997), and areal extent, but no volcanic landforms are evident in Mariner 10 images.

The volcanic history of Mercury is thus quite uncertain. Ground-based infrared and millimeter observations of Mercury have been interpreted as indicating a generally basalt-free surface, and thus a magmatic history governed primarily by intrusions rather than surficial eruptions of magma (Jeanloz et al., 1995). If this inference was correct, Mercury would have experienced less surface volcanism than any other terrestrial planet.

Correlated with the volcanic history of a planet is its thermal history, particularly the evolution of the thermal structure of the outer few tens of kilometers of the planet. Important constraints on that thermal evolution can come from observations of topography and gravity, because of the strong temperature dependence of the strength of crustal and mantle materials. For instance, the thermal gradient may be estimated from the flexural response of the planet's lithosphere to vertical loading by volcanic deposits or edifices (Solomon and Head, 1990). The pattern of tectonic features associated with the Caloris Basin has been interpreted as evidence that smooth plains deposits surrounding the basin loaded a lithosphere 75–125 km thick at the time of plains emplacement (Melosh and McKinnon, 1988), but gravity data are lacking to test this hypothesis. Additional constraints can come from gravity and topographic

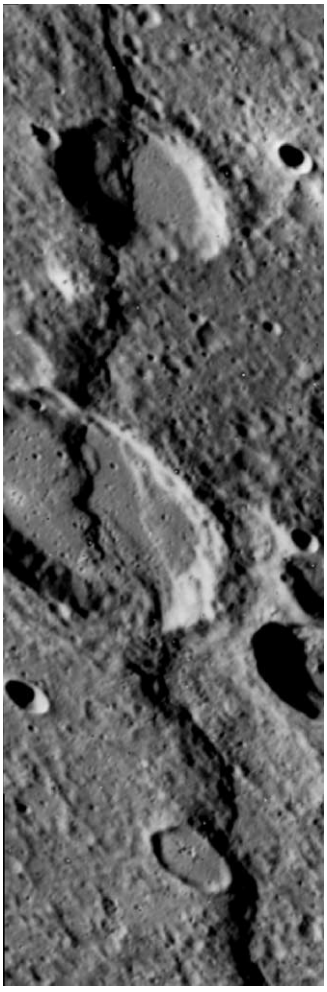

Fig. 6. A Mariner 10 image of Discovery Rupes, one of the longest and most prominent lobate scarps imaged by Mariner 10 (240 m/pixel).

measurements across impact structures, because the original topographic relief at the surface and at the crust-mantle boundary beneath such features may have been subject to viscoelastic relaxation of stress to a degree determined by feature age and the thermal evolution of the surrounding crust (Solomon et al., 1982).

The most prominent tectonic features on Mercury are the lobate scarps (Fig. 6), 20–500 km in length and hundreds of meters or more in height (Melosh and McKinnon, 1988; Watters et al., 1998). These scarps appear to be great thrust faults (Strom et al., 1975), although this interpretation should be tested with higher resolution images and topography. On the basis of their apparently random spatial and azimuthal distribution over the imaged fraction of the surface, Strom et al. (1975) surmised that the scarps record global contraction. From the number and height of the scarps, a total contraction of 1–2 km in radius was derived (Strom et al., 1975), a figure in agreement with global thermal history models for the cooling of the outer lithosphere or with partial solidification of a fluid metallic core (Solomon, 1976). Reconsiderations of both the geologically inferred (Watters et al., 1998) and geophysically predicted (Phillips and Solomon, 1997) magnitude of global contraction, however, have recently called this agreement into question. It has also been suggested that lobate scarps and older lineations preserve a record of tidal despinning, a process expected to yield a latitude-dependent pattern of fault type and orientation (Melosh and Dzurisin, 1978). Whether such a pattern is apparent in Mariner 10 images has been disputed (Melosh and McKinnon, 1988), but global mapping of tectonic structures would allow this hypothesis to be tested more rigorously.

The geologic history of the planet may require considerable revision once full global imaging coverage is available. Improved image resolution will permit the identification of key features diagnostic of plains emplacement mechanisms. Global stratigraphic and tectonic scenarios will be testable over the 55% of the surface yet unseen, and important new classes of landforms may be found. Earth-based radar observations of the portion of Mercury not seen by Mariner 10, for instance, show a radar-bright feature similar to large and relatively young shield volcanoes on Mars and Venus (Harmon, 1997). Such an identification, if verified by spacecraft observation, would demand models for interior thermal evolution different from those considered to date.

2.3. What are the nature and origin of Mercury's magnetic field?

Mercury's intrinsic magnetic field, discovered by Mariner 10, has a dipole component nearly orthogonal to Mercury's orbital plane and a moment of about $300\,nT - R_M^3$, where R_M is Mercury's mean radius (Connerney and Ness, 1988). This magnetic field is sufficient to stand off the average solar wind at an altitude of about $1\,R_M$ (Russell et al., 1988). The compression or erosion of the dayside magnetosphere to the point where solar wind ions can directly impact the surface remains a topic of controversy (Siscoe and Christopher, 1975; Slavin and Holzer, 1979a; Hood and Schubert, 1979; Goldstein et al., 1981).

The origin of Mercury's internal magnetic field is not well understood, yet the recent discoveries of a global field at Ganymede (Kivelson et al., 1996) and no global field on Mars (Acuña et al., 1998) heighten the importance of this question. Mercury's magnetic field cannot be externally induced, on the grounds that the measured planetary field is far greater in magnitude than the interplanetary field (Connerney and Ness, 1988). The possibility that the dipole field is a remanent field acquired during lithospheric cooling in the presence of an internal or external field has been suggested (Stephenson, 1976; Srnka, 1976), but such severe constraints on the timing and geometry of the remanence are required as to render the suggestion unlikely (Schubert et al., 1988). Short-wavelength magnetic field anomalies arising from regionally coherent remanent magnetization of crustal rocks remain a strong possibility, however. A

hydromagnetic dynamo in a liquid, metallic outer core is generally viewed as the most likely explanation of the dipole field (Schubert et al., 1988), although such other possibilities as a thermoelectric dynamo have been postulated (Stevenson, 1987). A better knowledge of the geometry of the magnetic field is needed to distinguish among these hypotheses.

Depending on the trajectory of the observing spacecraft, external sources can in fact dominate the total measured field, as was the situation for Mariner 10 (Ness et al., 1975, 1976). Errors from external fields were such that the uncertainty in Mercury's dipole moment is a factor of 2 (Slavin and Holzer, 1979b), and higher order terms are linearly dependent (Connerney and Ness, 1988). For these reasons, determining the structure of the magnetic field of Mercury must be carried out by an orbiting spacecraft that will accumulate long-term averages and remove the dynamics of the solar wind and Mercury's magnetosphere. These dynamic effects are readily identifiable by measuring simultaneously the plasma distribution and the magnetic field.

Mercury has a small magnetosphere with similarities to that of the Earth. Despite the limited duration of the two Mariner 10 flybys, which passed through the nightside magnetosphere for a total of only about 1 h, much was learned about its dynamics. Evidence of substorm activity was obtained in the form of intense energetic particle injections and dipolarizations of the magnetic field, similar to those observed in the near-tail region at Earth (Siscoe et al., 1975; Baker et al., 1986; Eraker and Simpson, 1986; Christon et al., 1987). Although the substorm interpretation has been questioned (Luhmann et al., 1998), compelling evidence was found for intense perturbation of the magnetic field due to field-aligned currents following substorm events (Slavin et al., 1997), in spite of the tenuous nature of Mercury's atmosphere and what may be a highly resistive planetary regolith. These magnetospheric dynamics are important in their own right and for comparison with those of the Earth, inasmuch as reconnection rates relative to 1 AU should be larger by a factor of three due to lower Alfvénic Mach numbers and a more intense interplanetary magnetic field (Slavin and Holzer, 1979a).

2.4. What are the structure and state of Mercury's core?

The hypothesis that Mercury's internal magnetic field arises from a core dynamo requires that Mercury have a metallic core that is at least partially molten. The presence of a fluid core during the time of Mercury's capture into its 3:2 spin-orbit resonance enhances the capture probability (Peale, 1988). However, different thermal history models of the planet lead to different predictions regarding the evolution and current state of the core. For most models in which core-mantle differentiation occurs early and the core is either pure iron or iron–nickel, an initially molten core should have cooled and solidified by now (e.g., Siegfried and Solomon, 1974; Fricker et al., 1976; Cassen et al., 1976). Schubert et al. (1988) show that a fluid outer core can be maintained to the present if a lighter element such as sulfur is mixed into the core to reduce the melting temperature.

A direct observation that yields an unambiguous determination of the existence and extent of a liquid core would have an important influence on theories for magnetic field generation and thermal history in terrestrial planets and icy satellites (Schubert et al., 1996), as well as for inferences on Mercury's rotational history. Such an observation, described by Peale (1976, 1981, 1988), is measurement of the amplitude of Mercury's forced physical libration. For the experiment to work, the fluid outer core must not follow the 88-day physical librations of the mantle, but the core must follow the mantle on the time scale of the 250,000-yr precession of the spin. These constraints lead to bounds on outer core viscosity, but the bounds are so broad as to be readily satisfied (a result robust with respect to the possible effects of topographic, gravitational, or magnetic coupling between core and mantle).

The physical libration of the mantle about the mean resonant angular velocity arises from the periodically reversing torque on the planet as Mercury rotates relative to the Sun. The amplitude of this libration ϕ_0 is approximately equal to $(B-A)/C_{\mathrm{m}}$, where A and B are the two equatorial principal moments of inertia of the planet and C_{m} is the moment of inertia of the solid outer parts of the planet about the rotation axis (Peale, 1972). Dissipative processes will carry Mercury to rotational Cassini state 1 with an obliquity θ close to 0° (Peale, 1988), which yields a relationship between θ and the differences in the moments of inertia and other orbital parameters. The moment differences also appear in expressions for the second-degree coefficients of the planetary gravity field, C_{20} and C_{22}.

These relations give a strategy for determining the presence of a fluid outer core and its outer radius by measurement of the second-degree gravity field, the obliquity θ, and the physical libration amplitude ϕ_0: $C_{\mathrm{m}}/C = [C_{\mathrm{m}}/(B-A)]\,[(B-A)/MR^2]\,[MR^2/C] \leqslant 1$. The first quantity in brackets follows from ϕ_0; the second is equal to $4C_{22}$; and the third can be obtained from the relation between θ and the second-degree gravity field coefficients. Thus C/MR^2 can be derived to an accuracy limited by the uncertainty in θ, and C_m/C can be obtained to an accuracy limited principally by the uncertainties in ϕ_0 and θ (Peale, 1997). If $C_{\mathrm{m}}/C = 1$, then the core of Mercury is solid; from a value for $C_{\mathrm{m}}/C < 1$ follows the radius R_{C} of the fluid outer core ($C_{\mathrm{m}}/C = 0.5$ for $R_{\mathrm{C}}/R = 0.75$), and from C/MR^2 the radius of any solid inner core may be estimated or bounded.

2.5. What are the radar-reflective materials at Mercury's poles?

Radar images of Mercury obtained in 1991 revealed regions of high reflectivity and high polarization ratios in

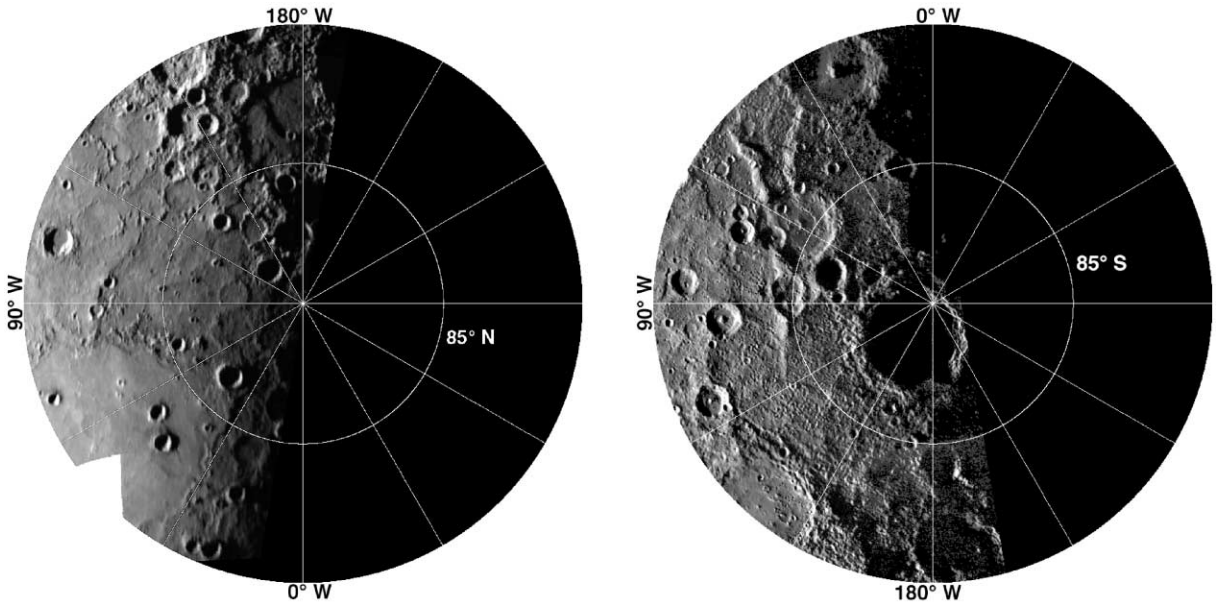

Fig. 7. North (left) and south (right) polar regions of Mercury, shown in orthographic projection at 1 km/pixel. The images are mosaics of north polar frames 156, 160, 164, and 165; and south polar frames 16621-23, 166626-29, and 166688-90. Shadowed craters at each pole are associated with radar-bright deposits (Harmon et al., 1994) thought to be volatile material in permanent cold traps. MESSENGER will determine the composition of these polar deposits.

Mercury's polar regions (Slade et al., 1992; Harmon and Slade, 1992). Because the high polarization ratios are similar to those of outer planet icy satellites and the residual polar caps of Mars, they are widely thought to indicate surface or near-surface water ice. A lower absolute radar reflectance than the Martian polar cap can be the result of incomplete areal coverage by ice units or a thin cover of dust or soil (Butler et al., 1993).

Because of the near-zero obliquity of the planet, the permanently shadowed floors of impact craters near the poles (Fig. 7) are sufficiently cold to preserve water ice for billions of years, given that Mercury has been in its current Cassini state for such a time (Paige et al., 1992; Ingersoll et al., 1992; Butler et al., 1993). Indeed, many of the areas of highest backscatter coincide with known impact structures imaged by Mariner 10 (Harmon et al., 1994). Such water ice is not likely to be the exposed portions of larger subsurface polar caps (Barlow et al., 1999), but impact volatilization of cometary and meteoritic material followed by random-walk transport to polar craters is a possible source for ice deposits (Killen et al., 1997; Moses et al., 1999).

Sprague et al. (1995) proposed the alternative hypothesis that the polar deposits are composed of elemental sulfur. Their rationale includes thermodynamic properties suitable for long-term stability in polar cold traps and several arguments for the presence of abundant sulfides in the regolith and interior of the planet. Sulfur could be injected into the atmosphere by sputtering, volatilization, or interior degassing and then redeposited in polar cold traps. Distinguishing between water ice and sulfur, an important step toward understanding volatile inventories in the inner solar system, can be accomplished through ultraviolet (UV) observations of the polar atmosphere and measurement of γ-ray spectra and neutron fluxes from the polar surface.

2.6. What are the important volatile species and their sources and sinks on and near Mercury?

Mercury's atmosphere is a surface-boundary exosphere whose composition and behavior are controlled by interactions with the magnetosphere and the surface. The atmosphere is known to contain six elements (H, He, O, Na, K, Ca), which together have a surface density at the subsolar point of 10^4 atoms cm^{-3} (Hunten et al., 1988). The Mariner 10 airglow spectrometer detected H, He, and O (Broadfoot et al., 1974, 1976), while ground-based spectroscopy revealed Na and K (Potter and Morgan, 1985, 1986) and recently Ca (Bida et al., 2000). Searches for additional constituents, e.g., Li (Sprague et al., 1996), have established only upper bounds. Ground-based studies of Na indicate that the atmosphere is spatially and temporally variable. Orderly changes in Na surface density are related to changes in solar radiation pressure (Smythe and Marconi, 1995), but atmospheric chaotic variations also occur (Killen et al., 1990).

Our inventory of Mercury's atmospheric composition is incomplete. Current understanding of source processes suggests the presence of yet undetected species, including Ar, Si, Al, Mg, Fe, S, and OH. With the exception of Ar, all of these species have strong ground-state emission lines

(e.g., Morgan and Killen, 1997) in the spectral range 0.13–0.43 μm. To date, observational constraints have prevented these species from being seen from the ground or Earth orbit.

The processes that supply and remove atmospheric material are poorly understood. Hydrogen and helium are thought to be primarily derived from neutralized solar wind ions, although photodissociation of meteoritic water yields some H and crustal outgassing should supply some He. Proposed sources for Na, K, Ca, and O include impact vaporization, ion sputtering, photon stimulated desorption, and crustal degassing. There is strong disagreement about the relative importance of these four mechanisms (McGrath et al., 1986; Cheng et al., 1987; Sprague, 1990; Morgan and Killen, 1997). The principal loss mechanisms are thermal escape and photoionization with subsequent loss through transport along open magnetic field lines. Although thermal escape appears to be the dominant loss mechanism for both H and He, it is probably unimportant for Na and K (Hunten et al., 1988). Magnetospheric processes, including ion precipitation onto Mercury's surface and pickup of photo-ions, may help control atmospheric sources and losses.

Determining a comprehensive inventory of atmospheric and magnetospheric species and measuring their spatial and temporal distributions will allow us to quantify the dominant source mechanisms for the various atmospheric species and will provide additional insight into upper crustal composition. Sputtering, for instance, can yield all the common regolith species in the atmosphere (O, Si, Ca, Al, Mg, and Fe). Impact vaporization preferentially supplies volatiles (S, H_2O, and OH; e.g., Killen et al., 1997) in addition to regolith species. Crustal diffusion is also predicted to contribute regolith-derived species to the atmosphere (Sprague, 1990). Plasma composition is important because of the close coupling among Mercury's surface, atmosphere, and magnetosphere. Both planetary and solar wind ions must be present at the bow shock, magnetopause, and cusps, and in the plasma sheet.

3. Scientific and measurement objectives for MESSENGER

The key questions discussed above, of central importance for improving our general understanding of the formation and evolution of terrestrial planets, lead to a set of scientific objectives for the MESSENGER mission and in turn to an instrument suite and measurement strategy. The scientific objectives for MESSENGER are to characterize (1) the chemical composition of Mercury's surface, (2) the planet's geological history, (3) the nature of Mercury's magnetic field, (4) the size and state of the core, (5) the volatile inventory at Mercury's poles, and (6) the nature of Mercury's exosphere and magnetosphere.

The first objective leads to a measurement requirement for global maps of major element composition at a resolution sufficient to discern the principal geological units and to distinguish material excavated and ejected by young impact craters from a possible veneer of cometary and meteoritic material. Information on surface mineralogy is also important. The second objective leads to the requirement for global monochrome imaging at hundreds of meters or better, for topographic profiles across key geological features from altimetry or stereo, and for spectral measurements of major geologic units at spatial resolutions of several kilometers or better. The third objective leads to a requirement for magnetometry, both near the planet and throughout the magnetosphere, as well as for energetic particle and plasma measurements so as to isolate external from internal fields. The fourth objective can be met by altimetric measurement of the amplitude of Mercury's physical libration as well as determination of the planet's obliquity and low-degree gravitational field. The fifth objective can be met by UV spectrometry of the polar atmosphere and by γ-ray and neutron spectrometry, imaging, and altimetry of polar-region craters. The sixth objective leads to measurement requirements for the identification of all major neutral species in the exosphere and charged species in the magnetosphere.

These measurement requirements are met for MESSENGER by a suite of seven scientific instruments plus the spacecraft communication system. There is a dual imaging system for wide and narrow fields-of-view, monochrome and color imaging, and stereo; γ-ray, neutron, and X-ray spectrometers for surface chemical mapping; a magnetometer; a laser altimeter; a combined UV–visible and visible-near-infrared spectrometer to survey both exospheric species and surface mineralogy; and a combined energetic particle and plasma spectrometer to sample charged species in the magnetosphere. Details on instrument design are given in a companion paper (Gold et al., 2001).

Answering all of the key science questions demands a Mercury orbiter. Characterizing the global planetary magnetic and gravitational fields and measuring the amplitude of Mercury's physical libration can be accomplished only from orbit. An orbiter enables multiple cuts through the magnetosphere and exosphere. Only an orbiter can provide sufficient integration time to produce elemental and mineralogical maps of the planet at the resolution necessary to distinguish among hypotheses for planet formation or to discern geological history. Overviews of the MESSENGER mission design and science implementation plans are given below.

4. Mission overview

The MESSENGER mission employs state-of-the-art chemical propulsion and multiple gravitational flybys to reach Mercury orbit. Both the flybys and the orbit have been optimized to satisfy all scientific measurement requirements within the constraints of the NASA Discovery Program. The selected mission combines the highest mass margin and the greatest schedule resiliency for this class of mission to Mercury for the coming decade.

Table 1
Flyby imaging coverage

Flyby	Phase angles, in/outbound	Flyby latitude, longitude	Illuminated longitudes	Coverage	High-resolution imaging, XRS, GRNS, VIRS targets
1	128°, 55°	0°, 324°W	83–263°W	Inbound: central part of Mariner-10 hemisphere, fill part of gore Outbound: Caloris, E part of unseen hemisphere	SW part of Caloris
2	135°, 37°	0°, 126°W	265–85°W	Inbound: central part of unseen hemisphere Outbound: W part of unseen hemisphere, fill remainder of Mariner-10 gore	Raphael, Renoir, Homer, Haystack Vallis

Table 2
Flyby imaging products and data volumes

Observation	Parameters	Uncompressed Mb	Compressed Mb
Movies	Approach/departure movies, 60 frames each, 6:1 compression	754	126
Departure mosaics	1 6×6 frame mosaic @ 800 m/px, 4:1 compression		
	1 10×10 frame mosaic @ 500 m/px, 4:1 compression	1741	435
Departure color	2 10-color images @ 9 km/px, 2:1 compression		
	2×2 frame 10-color mosaic @ 2.4 km/px, 2:1 compression	640	320
High resolution	100 frames, 4:1 compression	1280	320
Subtotal for immediate playback		4415	1201
Approach mosaic	4×10 frame mosaic @ 250 m/px, 4:1 compression	512	128
Approach color	10-color image @ 9 km/px, 4:1 compression	128	32
Imaging redundancy	2nd exposure at each frame position in departure monochrome mosaics	1741	435
High-resolution color	4×4 frame 10-color mosaic @ 1.2 km/px, 2:1 compression	2048	1024
High resolution	300 additional frames, 4:1 compression	3840	960
Subtotal for later playback		8269	2579
Total		12684	3780

Launched in March 2004 on a Delta 2925H-9.5 during a 20-day launch window, MESSENGER executes two gravity assists at Venus and two at Mercury. Orbit insertion is accomplished at the third Mercury encounter. The orbit has an initial periapsis altitude of 200 km and an initial latitude of periapsis of 60°N; the orbit is inclined 80° to the equatorial plane of the planet and has a 12-h period. The periapsis altitude and orbit phasing are optimized to balance thermal constraints against science requirements. The choice of inclination and latitude of periapsis is the result of a complex set of trade-space optimizations driven by imaging, altimetry, and radio science coverage requirements versus thermal input and mass. Solar perturbations impose changes in the periapsis altitude and latitude; periapsis altitude is corrected periodically in accord with science measurement requirements. The orbital phase of the mission will last one Earth year. Additional information on mission design is given by Santo et al. (2001).

5. Science implementation plan for MESSENGER

The MESSENGER mission is designed so that significant scientific return can be expected from each flyby, and the orbital phase of the mission will achieve all principal scientific objectives. During the first flyby, approximately half of the hemisphere not viewed by Mariner 10 will be illuminated; the first Mercury data return from MESSENGER will thus observe new terrain, including the previously unseen half of the Caloris Basin and its ejecta. During the second flyby, illumination will be centered on the eastern edge of the Mariner 10 hemisphere, including the site (58°N, 345°W) of the possible shield volcano imaged by radar (Harmon, 1997). Total flyby coverage will exclude only the polar regions and two ~20°-wide longitudinal bands, one ~120° west of Caloris and the other centered at ~140°W longitude in the Mariner 10 hemisphere. These gaps will be filled during the orbital phase of the mission. The two flybys have similar geometries (Table 1), and similar observation strategies will be used for each.

During the flyby phase, 85% of the planet will be imaged in monochrome at a resolution averaging ~500 m/pixel and in color at ~2.4 km/pixel (Table 2). Half of the planet will be covered in color at ~1.2 km/pixel. High-resolution data swaths will contain monochrome images at better than 125 m/pixel and visible-near-infrared and X-ray spectrometer transects with spot sizes of 700 m and 200 km,

Table 3
Orbital imaging coverage and data volumes

Observation	Parameters	Compressed Gb
Global monochrome map, nadir-looking	10% overlap downtrack, 20% overlap cross-track, 4:1 compression	4.7
Global monochrome map, stereo geometry	10% overlap downtrack, 20% overlap cross-track, 4:1 compression	4.7
Color gap-fill	40% of planet, 1.1 km/px, 10 filters, 2:1 compression	1.4
Color high-resolution	~1%, 5 filters, 300 m/px, 4:1 compression	0.1
High resolution	750 frames, 6:1 compression	1.1
Total		12.0

respectively. MESSENGER will also probe the atmosphere over two different regions and the magnetosphere along two different trajectories.

Important science investigations are also planned for the Venus flybys during the early part of the mission. For example, the imager will observe cloud layers at 415 and 950 nm to compare with the Galileo results (Belton et al., 1991), fields-and-particles instruments will observe pick-up particles (Williams et al., 1991), and the UV–visible spectrometer permits a search for changes in the composition of the upper atmosphere (Esposito, 1984). New science possibilities include a search for lightning on the nightside, altimetric probing of the Venus cloud deck, and a search for Venus's signature in X-rays, similar to that successfully conducted at comets (Lisse et al., 1996). The Venus flybys will also provide in-flight calibrations of instruments.

During the Mercury orbital phase of the mission, MESSENGER's science strategy will shift to detailed global mapping; characterization of the atmosphere, magnetosphere, and polar deposits; geophysical studies; and focused study of high-priority targets identified during the flyby phase. Details of the observations given in each investigation plan below follow from the key science questions.

5.1. Imaging investigation plan

The three major objectives of orbital imaging (Table 3) are filling gaps in flyby color coverage (Fig. 8), high-resolution targeted coverage (Fig. 9), and global stereo imaging for high-resolution topography. Filling gaps in color coverage is relatively simple except at low altitudes over high northern latitudes, when limiting smear requires short 30–50 ms exposure times. The impact on the signal-to-noise ratio (SNR) can be offset by pixel averaging, because full spatial resolution is ~120 m/pixel compared with the 1–2 km/pixel required to fill the gaps. High-resolution narrow-angle panchromatic images require ~2 ms exposure times to limit smear at periapse, which is easily attained with good SNR.

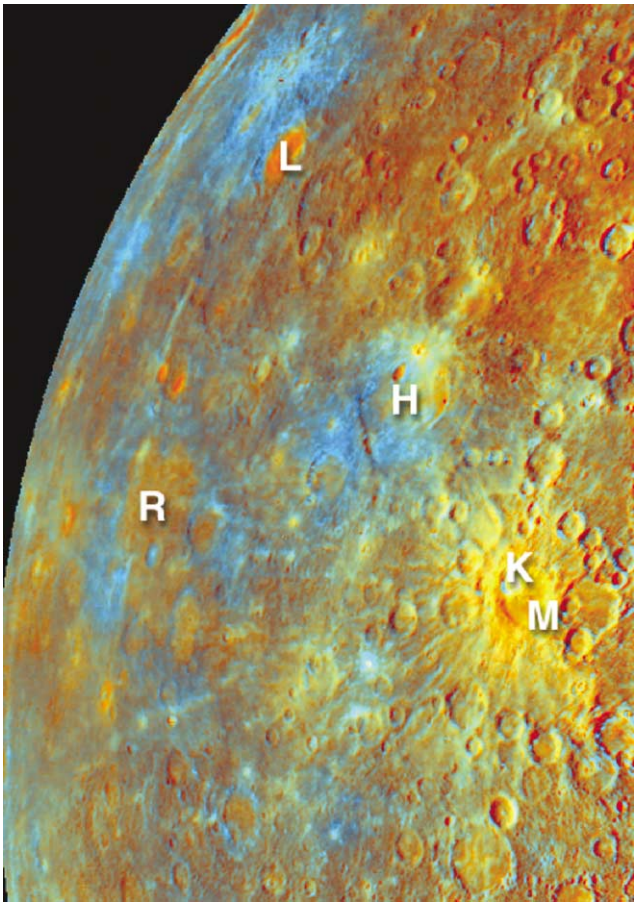

Fig. 8. Enhanced color composite showing portions of the incoming hemisphere of Mercury during the first Mariner 10 encounter (Robinson and Lucey, 1997). The red component is the inverse of the opaque index (increasing redness indicates decreasing opaque mineralogy), the green component is the iron-maturity parameter, and blue shows the relative visible color. The smooth plains unit covering the interior of the 120-km-diameter Rudaki crater (R) exhibits a distinct color from its surroundings and embaying boundaries consistent with material emplaced as a fluid flow. Both characteristics support the hypothesis that the plains are volcanic in origin. The blue material on the southwestern margin of Homer (H), a 310-km-diameter double-ring basin, exhibits diffuse boundaries, does not follow local topography, and is aligned along a linear segment of a basin ring, characteristics consistent with pyroclastic material. The blue deposit northwest of the 160-km-diameter crater Lermontov (L) is concentric to a small impact crater and may represent either pyroclastic deposits or material excavated by the impact and differing in composition from nearby surface material. The materials of the Kuiper-Muraski crater complex (K and M, respectively) have a very low content of opaque minerals. Kuiper (60 km diameter) is brighter and bluer than Muraski (125 km diameter), a difference likely attributable to different maturities.

Global monochrome image mosaics averaging 250 m/pixel (Fig. 10) will be built up using the narrow-angle imager for southern latitudes when altitude is high, and the wide-angle imager with its broadband filter for the

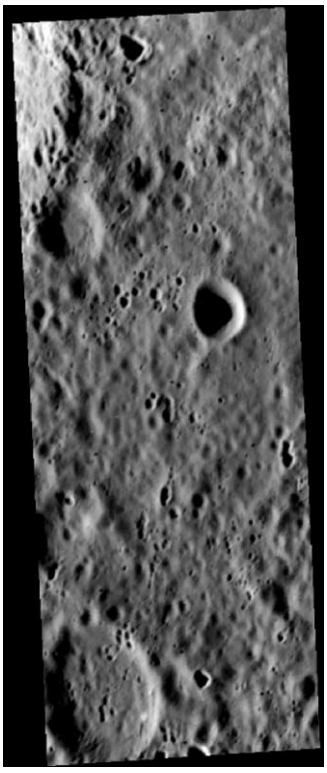

Fig. 9. One of the highest-resolution images of Mercury obtained by Mariner 10 on March 16, 1975, as the spacecraft made its third and final flyby of the planet. The image is an orthographic projection of frame 528922 (90 m/pixel). The frame is 68 km north-to-south and is centered at 9.7°S, 29.7°W, on the northeastern flank of the ejecta blanket of Kuiper, a relatively young impact crater (not shown) about 60 km in diameter. The highest-resolution images to be obtained by MESSENGER will be 25 m/pixel or better.

northern hemisphere (Fig. 11 and Table 4). At periapse the target resolution is exceeded by a factor of ~2. The one-year orbital mission encompasses two solar days on Mercury. A full global mosaic will be built up during the first 6 months of the mission. In the second 6 months, the operation will be repeated with different scan mirror positioning (Gold et al., 2001) to yield global stereo coverage (at ~250 m/pixel).

5.2. Elemental and mineralogical investigation plan

A γ-ray and neutron spectrometer will yield global maps of Mercury's elemental composition. The γ-ray spectrometer detects discrete-line γ-ray emissions and will be used to measure galactic-cosmic-ray excited elements O, Si, S, Fe, and H and naturally radioactive elements K, Th, and U to a depth of about 10 cm (Trombka et al., 1997). The neutron spectrometer component detects low-energy neutrons produced by cosmic-ray bombardment and moderated by collisions with near-surface (~40 cm), H-rich material (Feldman et al., 1997). Since solar illumination does not significantly affect γ-ray or neutron coverage, observations over the poles will detect any concentrated water ice (H and O) or sulfur (S) deposits in the permanently shadowed regions. For example, H can be detected by the 2.223 MeV γ-ray line and by study of line strengths due to capture and inelastic scattering of neutrons (Evans and Squyres, 1987). Simultaneous measurement of the thermal and epithermal neutron flux yields strong constraints on the hydrogen content of the regolith. The best determination of the amount of hydrogen present can be made by a self-consistent modeling of both the γ-ray spectrum and neutron-flux measurements (Haines and Metzger, 1984a, b). For an assumed composition, we have calculated (Table 5) the compositional uncertainty for a given counting time for the instrument described by Gold et al. (2001). MESSENGER will be able to discern a high sulfur content, if present (Table 5). The spatial resolution will be about 170 km from 200 km altitude, and the spacecraft will be over the north polar region for ~15 min every orbit (once every 12 h).

Ultraviolet, visible, and near-infrared spectrometry will be used to search for ferrous-bearing minerals (absorption bands near 1 μm), Fe–Ti bearing glasses (spectral signatures near 0.34 μm), and ferrous iron (strong absorption band near 0.25 μm) on the planet's surface. These measurements will be made with a spatial resolution of 5 km or better and will be acquired simultaneously with imaging sequences.

X-ray spectrometry remotely senses characteristic X-ray emissions, which are diagnostic of elemental composition within 1 mm of the surface. With a planet-pointing X-ray spectrometer, we will detect characteristic X-rays to measure globally the surface abundances of elements Mg, Al, Si, Ca, Ti, and Fe with spatial resolution down to ~20 km. To ensure a proper quantitative analysis, a sunward-pointing X-ray detector will measure the time-variable incident solar flux.

The X-ray measurements complement those from γ-ray and neutron spectrometry. For the same element, differences in measured concentrations should reveal the extent of surface processing and allow comparison with elements sputtered from the surface. X-ray, neutron, and γ-ray measurements also provide an independent calibration of the mineralogical identifications made from absorption bands. Table 6 lists the required integration times for identifying the listed elements at the 10% uncertainty level for different solar conditions for the MESSENGER instrument configuration (Gold et al., 2001). The orbital phase of the mission will provide ~180 h (7.6 d) of high-resolution X-ray measurements at high northern latitudes.

5.3. Magnetic field investigation plan

To characterize Mercury's magnetic field, emphasis early in the mission will be on periapsis passes (<1000-km altitude), where the planetary contribution to the ambient field is greatest. These measurements will remove the present ambiguity in the multipole parameters (Connerney and Ness, 1988).

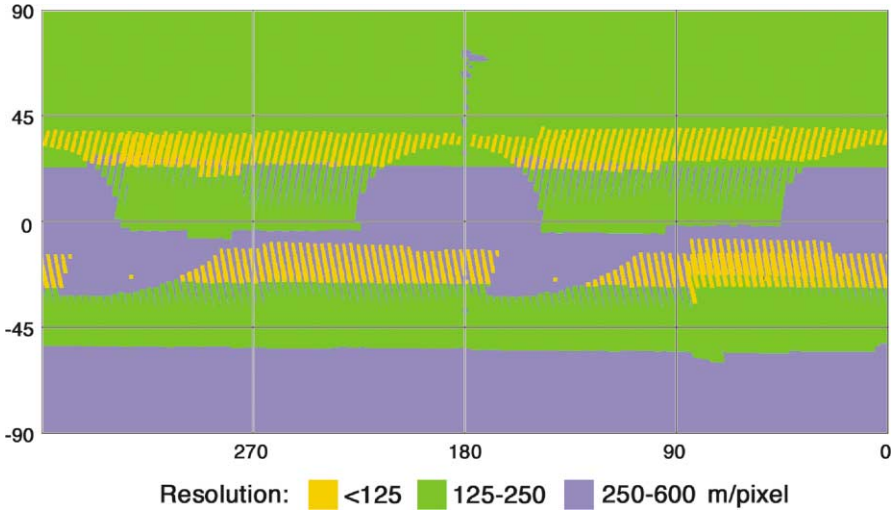

Fig. 10. Anticipated spatial resolution of MDIS images of Mercury at the end of global mapping in MESSENGER's orbital phase (cylindrical equidistant projection). Image resolutions are lower in the southern than the northern hemisphere because of the elliptical MESSENGER orbit. Most locations are imaged at low emission angles, i.e., nadir-pointed, which are ideal for cartography. Exceptions are the two polar regions and the equatorial regions near 0° and 180°W longitude, which are imaged at up to 35° off-nadir. The greater line-of-sight distances with such an off-nadir geometry for these locations decreases only slightly the resolution of the resulting images.

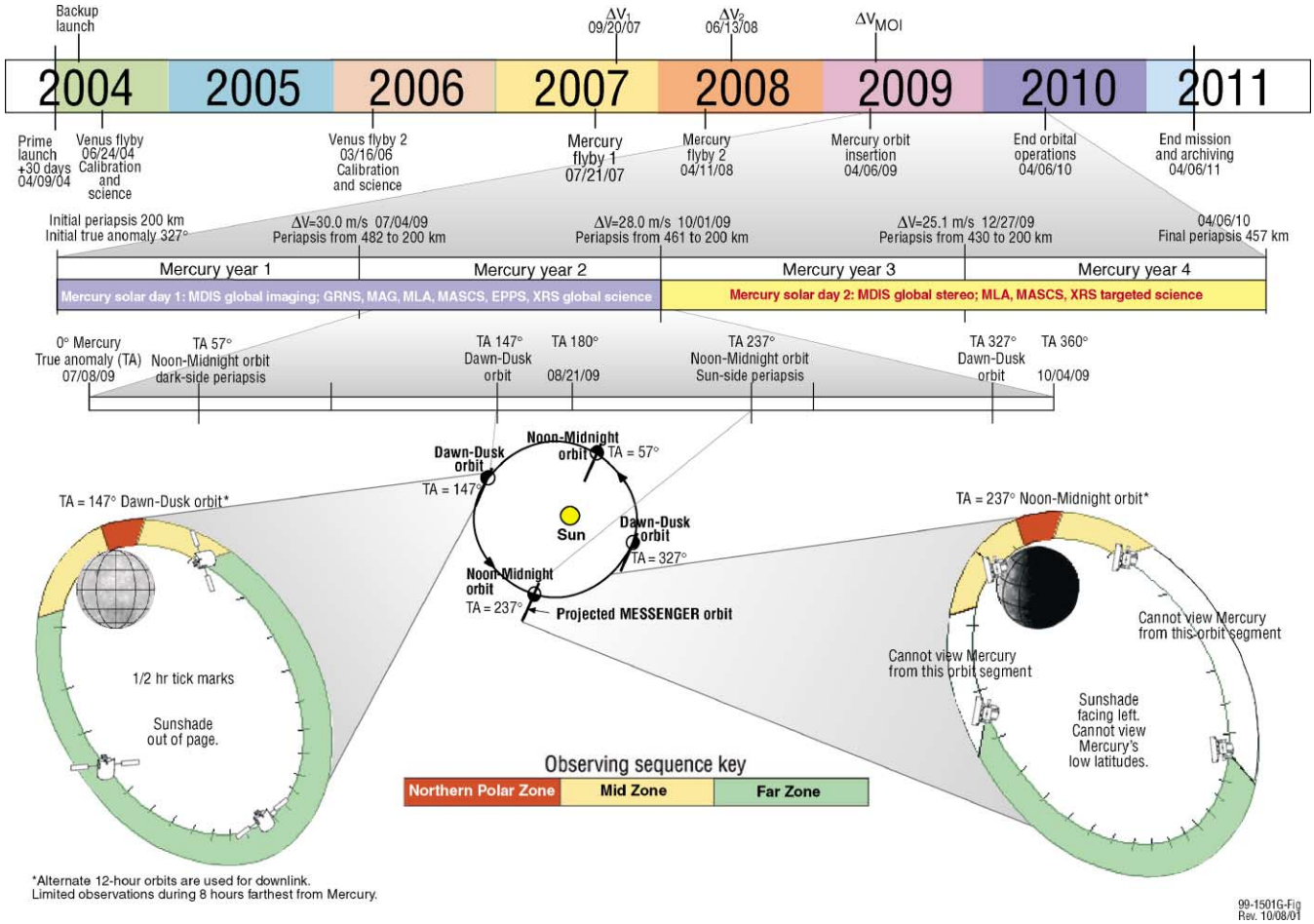

Fig. 11. The MESSENGER mission timeline. The top line shows all significant events from mission launch through end of mission and data archiving. ΔV_1 and ΔV_2 are deep-space propulsive maneuvers and ΔV_{MOI} is the propulsive burn at Mercury orbit insertion (Santo et al., 2001). The second line provides further details for the orbital phase of the mission. The third line expands on Mercury year of observations, from perihelion to perihelion. The accompanying figure at the center shows the progression of the orbit in local time. Observing strategies are detailed for a dawn-dusk (terminator) orbit ($\mathrm{TA} = 147^\circ$) at lower left and a noon-midnight orbit ($\mathrm{TA} = 237^\circ$) at lower right. The divisions of these orbits by observing sequence are keyed to the columns in Table 4.

Table 4
MESSENGER orbital observation strategy

Instrument		Northern Polar Zone	Mid Zone	Far Zone
MDIS	NA	—	Mapping, <125 m/pixel	Mapping, <500 m/pixel
	WA	Mapping, <125 m/pixel	Mapping, <500 m/pixel	Mapping, <1000 m/pixel
GRNS		300-s integration time	500-s integration time	1800-s integration time
XRS		100-s integration time	300-s integration time	2000-s integration time
MAG		10-Hz sampling	1-Hz sampling	0.1-Hz sampling
MLA		2.5-Hz ranging (up to 1000 km altitude)		Standby
MASCS	VIRS	~1-s integration surface observations		
	UVVS	—	<100-s integration limb scans, ~1-s surface observations	
EPPS		EPS — 36-s integration time; FIPS — 1-min scan time		
Radio science		Radiometric data 8 h/day over various portions of orbit		

Table 5
Compositional uncertainty for given γ-ray observation times

Element	Energy (keV)	Line type	Assumed composition[a] (%)	Uncertainty for 1-h integration (%)	Uncertainty for 8-h integration (%)
O	6129	I	45.3	6.85	2.42
Mg	1369	I	22.6	2.13	0.75
Mg	3918	C	22.6	27.87	9.86
Si	1779	I	21.5	2.21	0.78
Si	3539	C	21.5	11.95	4.22
Fe	847	I	2.3	0.48	0.17
Fe	7640	C	2.3	1.02	0.36
Al	2210	I	3.0	2.67	0.94
Al	7724	C	3.0	17.06	6.03
Ti	983	I	1.0	1.27	0.45
Ti	6761	C	1.0	0.48	0.17
Ca	3737	I	4.0	4.98	1.76
Ca	1943	C	4.0	10.80	3.82
K	1461	N	1.2×10^{-1}	1.35×10^{-2}	4.78×10^{-3}
Th	2614	N	2.0×10^{-4}	6.05×10^{-5}	2.14×10^{-5}
Polar regions, enhanced sulfur case (10% sulfur by weight assumed)					
S	2230	I	10.0	3.39	1.20
S	5424	C	10.0	4.74	1.68
Polar regions, enhanced hydrogen case (9% water ice by weight assumed)					
H	2223	C	1.0	0.18	0.06

[a]Weight percent, from Brückner and Masarik (1997). I = inelastic scatter, C = capture, N = natural radioactivity. Uncertainties are at the 3-σ level.

To produce a three-dimensional model of Mercury's magnetosphere, magnetic field measurements will be taken at low sample rate over the entire magnetospheric fraction of the orbit (Fig. 12 and Table 4), with high-rate samples at the magnetopause, cross-tail, and field-aligned external current regions. These observations will be combined with charged particle observations to investigate such dynamic processes as substorms and magnetic reconnection at the magnetopause. With apparent substorm durations of only about 1 min at Mercury, it should be possible to gather definitive substorm statistics at a variety of locations throughout the magnetosphere without the motion of the spacecraft aliasing measurements.

Mercury's magnetosphere contains a charged particle population that varies significantly on short temporal (~10 s) and spatial scales. Nothing is known from the Mariner 10 flybys regarding the compositions of these particles, and there remains controversy about the interpretation of Mariner 10 data (Armstrong et al., 1975). To answer these questions, an energetic particle and plasma spectrometer will be operated continuously in concert with the magnetometer. Representative samples of the global particle distribution in the magnetosphere will be obtained during each Mercury

Table 6
X-ray observation times[a]

Element	Assumed abundances	Proportional counter with 95% background rejection		Proportional counter with 75% background rejection	
		Normal	Flare	Normal	Flare
Fe	2.3%	—	80 s	—	2 min
Ti	1.0%	—	3 min	—	4 min
Ca	4.0%	—	10 s	—	30 s
Si	21.5%	7 min	2 min	18 min	3 min
Al	3.0%	2 h	22 min	8 h	50 min
Mg	22.5%	5 min	2 min	11 min	3 min

[a]Counting times are those required to reproduce the assumed composition at the 10% uncertainty level using three balanced-filter, multi-wire proportional counters of 10-cm^2 active area each. Assumed abundances, in weight percent, are from Brückner and Masarik (1997). Count rates are scaled from actual measurements made by NEAR Shoemaker at Eros in July 2000 (1.78 AU) to the assumed composition at Mercury (at 0.387 AU).

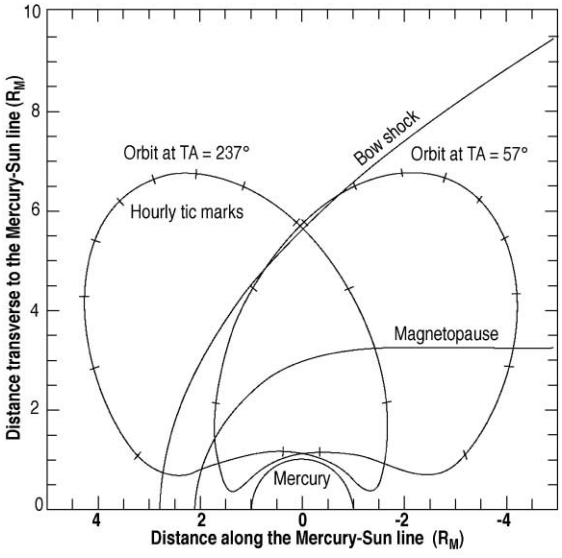

Fig. 12. MESSENGER coverage of the Mercury magnetosphere during the two noon-midnight orbits (Mercury true anomaly 57° and 237°); tic marks are spaced 1 h apart. MESSENGER will provide excellent coverage of the interactions at the Mercury bow shock and magnetopause (approximate locations shown) along with good substorm coverage in the close-in magnetotail.

year. We will also monitor background-penetrating particles to provide a measure of radiation dosage for spacecraft and instrument electronic subsystems.

5.4. *Libration amplitude, altimetry, and gravity investigation plan*

The laser altimeter will measure the range to the surface of Mercury at spacecraft elevations of 1000 km or less with at least 90% probabililty of detection and lower detection rates at higher altitudes. To determine range, the spacecraft orbital trajectory will be interpolated to times of measurement, correcting for spacecraft pointing. Ranges will be converted to planetary radii with respect to Mercury's center of mass. Profiles will have an along-track resolution of 0.8–1 km. The MESSENGER orbit will enable altimetric mapping of nearly the entire northern hemisphere. Topographic profiles will be assembled into regional grids at resolutions dictated by ground-track spacing. Radii obtained from altimetry in the northern hemisphere and radio occultations in the northern and southern hemispheres (Fig. 13) will be combined to produce a model of Mercury's global shape. The combination of topography with gravity and compositional information will be used to model interior density variations, particularly the distribution of crustal thickness.

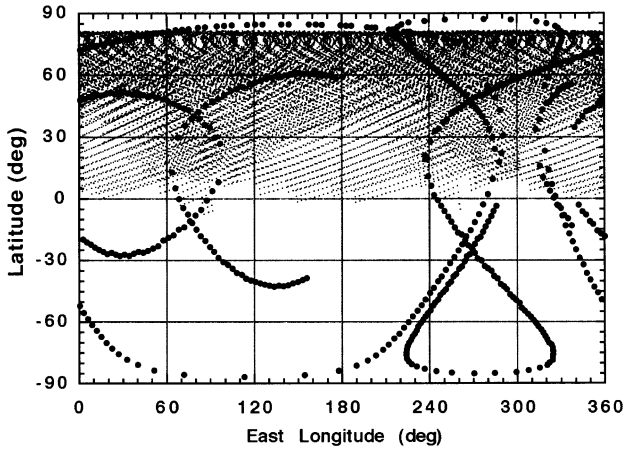

Fig. 13. Locations of potential radio occultations (large dots) and representative altimetry footprints (small dots) during MESSENGER's orbital phase. Planetary radii from altimetry in the northern hemisphere and occultations in both hemispheres will be combined to produce a model of Mercury's global shape and to solve for the amplitude of Mercury's physical libration.

Mercury's forced physical libration will be manifest as an irregular rotation of the planet, i.e., a 350-m half-amplitude oscillation in longitude with a period of 88 days (one Mercury year). We will extract the libration from the rotation using the planetary topographic and gravitational shape (Zuber and Smith, 1997). Others have proposed recovering this signal using short-wavelength horizontal offsets measured with an orbital camera (Wu et al., 1995, 1997). The MESSENGER method offers a similar level of predicted recoverability with a much lower data rate and simple data processing.

Libration recovery from topography requires knowledge of the longest-wavelength longitudinal terms (spherical-harmonic orders 1–4) referenced to the planetary center of mass. In addition, we must determine the precise position of the planetary rotation pole. Our approach will be to use altimetry, occultation, and gravity data to solve for the libration's amplitude and phase, the direction of the spin axis (obliquity), and the low-degree planetary

Table 7
Expected accuracies for second-degree gravity field coefficients and rotation pole position

Gravity field	Complete to degree and order 16 $\sigma(C_{20}) < 0.4\%$, assuming $C_{20} = -2.7\times10^{-5}$ $\sigma(C_{22}) < 1\%$, each coefficient, assuming $C_{22} = 1.6\times10^{-5}$	
Pole location	Right ascension of the pole	$<1.4\times10^{-4}$ rad
	Declination of the pole	$<1.8\times10^{-4}$ rad
Spacecraft orbit	Along-track error	~50 m
	Across-track error	~20 m
	Radial error	~5 m

Table 8
Principal perturbations to node of spacecraft orbit

Source of perturbation	Type	Magnitude
Mercury gravity		
$C_{20} = -2.7\times10^{-5}$	Secular	34 km
$C_{21} = 1.0\times10^{-7}$	Periodic, 59 days	10 m
$C_{22} = 1.6\times10^{-5}$	Periodic, 30 days	210 m
Solar radiation pressure	Secular	200 m
	Periodic, 88 days	400 m
Physical libration	Periodic, 88 days	<350 m

altimetric and gravitational shapes. Since knowledge of only the long-wavelength shape is required, the sparse data distribution in the southern hemisphere provided by the occultations will be adequate.

To demonstrate that MESSENGER can measure the libration to the required accuracy, we have carried out a preliminary simulation of the recovery of the signal for a mission scenario similar to that adopted (Santo et al., 2001). Altimeter data were simulated at 1-min intervals (the actual data rate will be 1–5 Hz). We assumed 10-m radial noise due to altimeter measurement and orbit errors and 0.1° noise from spacecraft pointing error. Normal equations were developed from the simulated data, and we solved for the libration, the spin-axis direction, and spherical-harmonic topographic model expanded to degree and order 16. Free adjustments were permitted for the libration and the spin axis, but a standard deviation (σ) of 100 m was applied to each coefficient of the 16×16 topography. From the altimetry data, we recovered the libration amplitude to 9% ($1\,\sigma$) and the pole position to $(1–2)\times10^{-5}$ rad. The simulation demonstrates the ability to recover the libration and obliquity to a 10% level, sufficient for discrimination of a liquid from a solid core. Independent estimates of libration amplitude and obliquity can be obtained from the gravity field, although for the assumptions made for the simulation the recovered pole position is not as precise (Table 7).

The X-band transponder on the spacecraft will provide range-rate data between the spacecraft and a Deep Space Network (DSN) ground station and will be used to derive a spherical harmonic expansion of Mercury's gravity field. From a simulation of the spacecraft orbital evolution over the mission life, we estimate that a gravity model to degree and order 16 will be recoverable with an average resolution of ~400 km in the northern hemisphere and about 1500 km in the southern hemisphere. The principal perturbations over one Earth year of the node of the spacecraft orbit are given in Table 8. Particularly important are the very low-degree terms because of their relationship to the libration. Table 7 shows the ability to estimate the second-degree terms and the direction of the rotation pole from tracking the orbiting spacecraft over one Earth year.

For a period during most orbits the spacecraft will be occulted from Earth. If the spacecraft is tracked into, or as it emerges from, occultation, the time of the occultation can be used to estimate the planetary radius at the grazing ray location (Kliore et al., 1972; Lindal et al., 1979). Since the orbital position will be known to a few tens of meters we can derive occultation radii to a similar level. Measurements will be particularly important in the southern hemisphere, which will lack altimetric coverage (Fig. 13). These observations will be very important in constraining the global shape of the planet (e.g., Smith and Zuber, 1996) and will significantly improve our knowledge of the offset between centers of figure and mass for Mercury (Anderson et al., 1996).

Combined altimetry and radio tracking data will provide the basis for a global geodetic control network with which to reference other data sets, particularly imaging. The network will have a precision of ~50 m horizontally and 10 m radially in the mid to high northern latitudes. Areas of poorer quality topographic information in the southern hemisphere where altimetry is lacking will be filled in with occultation radii and a co-registered global image-based control network.

5.5. *Exosphere, magnetosphere, and polar volatiles investigation plan*

Spectrometry from 0.115 to 0.600 μm (at 1-nm resolution) will be used to measure altitude profiles of known species (H, O, Na, K, and Ca) and to search for predicted species not previously detected (Si, Al, Mg, Fe, S, OH) as well as new species. Limb scans will be made by "nodding" the spacecraft to provide altitude profiles of emission lines. Ground-based studies indicate that an altitude resolution of 25 km and a latitude resolution of better than 20° are required to characterize the exosphere adequately.

Species in the exosphere–magnetosphere system are diagnostic of volatiles present on the surface (Cheng et al., 1987). Surface sources of exospheric materials will be mapped with the X-ray, γ-ray, and neutron spectrometers, and the magnetospheric connection will be made with measurements of energetic ions, electrons, and thermal plasma ions. In

addition to magnetospheric ions, solar-wind pick-up ions, e.g., Na^+ and K^+, that originate as neutral atoms at Mercury and are ionized locally will be measured. The γ-ray and neutron spectrometer in concert with laser altimetry will be used to characterize the composition and thickness of frozen volatiles in permanently-shadowed craters near Mercury's poles, postulated to be responsible for the anomalous radar returns from those regions (Slade et al., 1992; Harmon et al., 1994).

5.6. Gravitation and general relativity investigation plan

Although not specific objectives of the MESSENGER mission, improvements to our understanding of gravitational physics and tests of general relativity are areas where potential gains can be made on a best-effort basis to improve on current estimates of several fundamental physical parameters. Ranging to the MESSENGER spacecraft will enable knowledge of Mercury's center of mass to 10 m, an improvement of more than an order of magnitude. This gain in precise positioning will result in improvements in Mercury's orbital elements and perihelion shift (Shapiro et al., 1972) that could be used to revise estimates of the Parameterized post-Newtonian (PPN) parameters β and γ (Reasenberg et al., 1979; Lebach et al., 1995) as well as the solar flattening, J_2.

In practice, both general relativity and J_2 contribute to the precession of Mercury's perihelion, with the relativistic effect exceeding that from J_2 by about a factor of order 10^4. Improving measurement of the orbital precession will provide a tighter constraint on the PPN combination $(2+2\gamma-\beta)$ obtained by radar range measurements to Mercury (Shapiro et al., 1972). Also of interest would be an improved estimate for the relativistic time delay, which is proportional to $(1+\gamma)$. This quantity, obtained from ranging to the Viking spacecraft at Mars (Reasenberg et al., 1979) and from Very-Long-Baseline Interferometry observations of radio emission from quasars along ray paths close to the Sun (Lebach et al., 1995), currently has a relative accuracy of 2×10^{-3}.

6. Instrument suite

The challenge of providing the full set of measurements required to satisfy the MESSENGER science objectives is met with a suite of seven instruments, along with the spacecraft telecommunications system. These instruments include the Mercury Dual Imaging System (MDIS) with both wide-angle (WA) and narrow-angle (NA) imagers, a Gamma-Ray and Neutron Spectrometer (GRNS), an X-Ray Spectrometer (XRS), a Magnetometer (MAG), the Mercury Laser Altimeter (MLA), the Mercury Atmospheric and Surface Composition Spectrometer (MASCS), and the Energetic Particle and Plasma Spectrometer (EPPS). The MASCS includes both an Ultraviolet-Visible Spectrometer (UVVS) and a Visible-Infrared Spectrograph (VIRS). Details on instrument characteristics, performance, and placement on the spacecraft are given by Gold et al. (2001).

The payload instrumentation has been selected to provide functional redundancy across scientific objectives to give complementarity of observations in case of problems. Such redundancy also provides for important consistency checks of results obtained with more than one instrument. The redundancies include:

- Surface chemistry (GRNS, XRS, VIRS)
- Geological features (WA imager, NA imager)
- Surface spectral properties (WA imager; UVVS, VIRS)
- Altimetry and planetary shape (MLA, stereo imaging, radio occultations)
- Atmospheric properties (UVVS, EPPS)
- Polar deposit composition (GRNS, EPPS)

7. Mission observing profile

The observing profile for the MESSENGER mission is driven by tradeoffs among required observations, thermal constraints, and mass and downlink limitations. Investigation plans that link the science measurement objectives to the instrument requirements have been given above. Characteristics of the spacecraft trajectory and orbit are discussed in a companion paper (Santo et al., 2001).

With orbital operations at Mercury extending for one Earth year, Mercury will make four revolutions about the Sun during the mission's orbital phase. Four Mercury years are required for measuring the planetary libration, and the planet's 3:2 spin resonance means that MESSENGER's orbital phase extends for two Mercury solar days (Fig. 11). This duration allows for global surveying during the first six months followed by stereo coverage, concentrated observations of targets of interest, and repeat coverage as required. A one-Earth-year orbit phase also improves the accuracy of surface composition measurements.

MESSENGER enters its orbit over the planet's terminator at a Mercury true anomaly (TA) of 327°. (0° TA labels Mercury's azimuthal position in orbit at the time of its perihelion.) The orbit remains fixed in inertial space due to Mercury's small oblateness. Thus, with no additional use of fuel, this orbit minimizes the thermal stresses experienced by the spacecraft. Fig. 11 shows the evolution of MESSENGER's observing geometry during one Mercury year of operations (July 8, 2009, through October 4, 2009). Color coding indicates the various observing zones and instrument operation plans for the two extreme cases: near-terminator (dawn-dusk) orbit (TA 147° or 327°) and near-noon-midnight orbit (TA 57° or 237°). Thermal stresses for TA 57° are less than for TA 237°, because MESSENGER's altitude over the sub-solar point is higher (4426 km) in the former case.

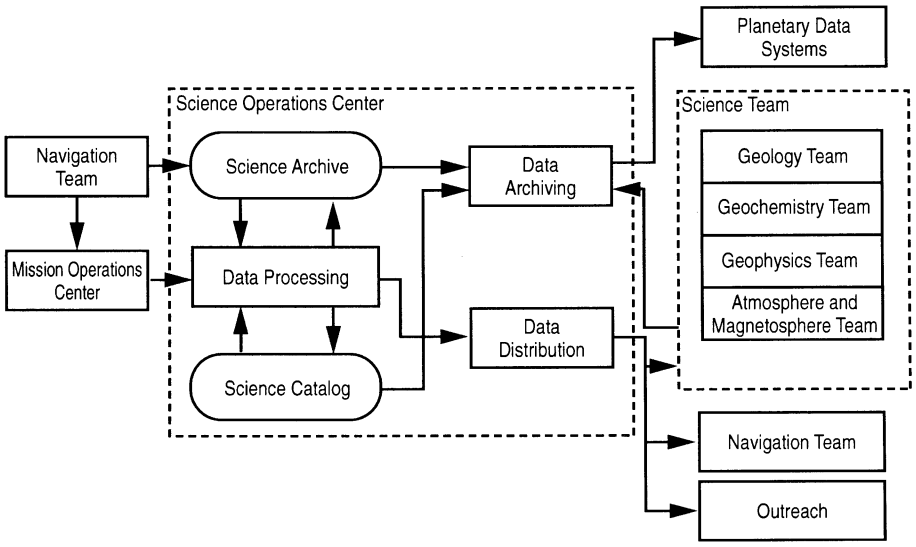

Fig. 14. Schematic view of science data flow during the MESSENGER mission.

MESSENGER orbits Mercury twice per 24 h. Science observations (Fig. 11) are made during the first 12-h orbit; for 8 h of every second 12-h orbit (not shown) the spacecraft is oriented for data downlink to Earth and acquisition of ranging data. When in near-terminator orbits, the spacecraft continuously rolls about the Sun line to keep the planet in nadir view. In near-noon-midnight orbits, the spacecraft maneuvers to the extent possible to maximize the coverage of the planet while maintaining the spacecraft bus behind the sunshade (Santo et al., 2001).

The Mercury flybys will be used to obtain imaging difficult to achieve during the orbital phase. The flyby observation strategy and data downlink plan are driven by the flyby geometry (Table 1). Science and calibration data from the Venus flybys and during cruise use low data rates. MDIS performance measurements, spacecraft radioisotope buildup by cosmic rays (GRNS), and spacecraft magnetic field (MAG) data are the only required data prior to first Mercury flyby; other science data will be collected as resources permit.

8. Data analysis and archiving

All relevant mission data will be validated by the project and archived to the Planetary Data System (PDS). Where possible, software code and design are being reused from previous programs, in particular Near Earth Asteroid Rendezvous (NEAR) Shoemaker, but will be retested and validated by the project. New software for MESSENGER is being developed and tested using formal software development methods and will be overseen by the project.

All MESSENGER data will be downlinked to the DSN and forwarded to the Mission Operations Center (MOC) at The Johns Hopkins University Applied Physics Laboratory (JHU/APL). Telemetry data will flow from the MOC to the Science Operations Center (SOC) for low-level data processing, data distribution, and archiving (Fig. 14). The SOC will create and maintain a Science Archive, the central repository for science data products; it will maintain a telemetry archive, a record of instrument and spacecraft commands, and records of science sequences; it will clean, merge, and time-order science telemetry and separate it by instrument; and it will develop and maintain a Science Data Catalog, to enable easy access to science data files, to support creation of data products, and to facilitate data searching. The SOC will also perform preliminary data calibrations, using algorithms developed by the Science Team.

Table 9 illustrates the MESSENGER data products and the teams responsible for producing them. EPPS and MAG products will be in the form of time series. Spectra from

Table 9
MESSENGER data products

System	Data product	Team	Lead
Spacecraft	Uncalibrated telemetry	SOC	—
Spacecraft	Command history	MOC	—
Instruments	Calibrated instrument data	SOC	—
MDIS	Catalogued images	GG	Murchie
GRNS	γ-ray spectra, neutron flux	GC	Boynton
XRS	X-ray spectra	GC	Trombka
MAG	**B**-field vectors	AM	Slavin
MLA	Range profiles, radiometry	GP	Zuber
MASCS	Spectra, tangent height	AM	McClintock
EPPS	Energy spectra, composition, and distribution functions	AM	Gold
Radio Science	Doppler data, ranging data, occultation times	GP	Smith

GRNS, MASCS, and XRS will be organized by latitude and longitude. Preliminary data will be released on a public web site within ~72 h of downlink. All data, applicable housekeeping, and calibration algorithms will be released to the PDS after the second flyby and within 6 months of the end of mission. The Science Team is responsible for determining the general layout of the archive, the SOC is responsible for producing original media for the PDS, and the PDS is responsible for making copies and distributing the archive. Public dissemination of selected images and data will occur immediately following calibration with the best currently available calibration algorithms. Selected additional data products of scientific interest will be disseminated in electronic and printed formats.

A Data Working Group (DWG) consisting of the Principal Investigator (PI), Project Scientist, and Science Group Chairs (see below) oversees calibration and data product software development. The DWG provides configuration oversight of all software implementations to ensure that data delivered to the PDS are produced using project-approved software.

The science data processing facilities are being developed by the Data System Coordinator in cooperation with the Science Team. The facilities will share a common architecture and will be at JHU/APL and operated by Applied Coherent Technologies, Inc., a MESSENGER team partner. The SOC is designed to ingest the total science and housekeeping stream from the DSN on a daily basis during MESSENGER orbital operations, process data for the data analysis facilities, and produce data products for archiving with the PDS.

None of the MESSENGER data will be treated as proprietary. We recognize the necessity and responsibility for providing fully documented data sets in a timely manner to maximize the scientific return from the mission. Optimal use will be made of the PDS and the World Wide Web to provide results to the scientific community as well as to associated educational and outreach endeavors.

9. Science team organization

The MESSENGER Science Team includes all of the authors of this paper. In accordance with the guidelines of the NASA Discovery Program, the Science Team is headed by the PI, S. C. Solomon, who has overall responsibility for the design, execution, and success of the mission. To facilitate the design, development, and testing of instrumentation, and to carry out the analysis of mission data in an effective manner, the Science Team is divided into four broad groups with distinct but complementary interests. A Geology Group (GG), chaired by J. W. Head, oversees development of the imaging system and will lead the scientific interpretation of the data pertinent to the geological history of Mercury. A Geochemistry Group (GC), chaired by W. V. Boynton, oversees development of the γ-ray, neutron, and X-ray spectrometers and the VIRS and will lead the scientific interpretation of the measurements on the surface composition of the planet. A Geophysics Group (GP), chaired by M. T. Zuber, oversees development of the altimeter and the spacecraft transponder system, and will lead the scientific interpretation of altimetry and gravity measurements, including the measurement of Mercury's physical libration and its relation to the state of the core and the origin of the magnetic field. An Atmosphere and Magnetosphere Group (AM), chaired by S. M. Krimigis, oversees development of the magnetometer, UVVS, and EPPS, and will carry out the scientific analysis of magnetic field structure, neutral atmosphere, and energetic particle and thermal plasma characteristics. These Chairs, together with the Project Scientist, R. L. McNutt, Jr. the Science Payload Manager, R. E. Gold, and the Project Manager, M. R. Peterson, constitute the Science Steering Committee (SSC). The PI leads the SSC in overseeing the entire MESSENGER mission science implementation, from instrument development through the interdisciplinary synthesis of all data sets.

10. Current status

As of this writing, the MESSENGER project is in its preliminary design phase (Phase B), on schedule and on budget for a March 2004 launch. Ongoing design and trade studies will continue to sharpen the specifics of mission design and spacecraft and instrument implementation. The principal goal of these studies is to minimize mission risk while maintaining or enhancing the capability to achieve all of the scientific objectives for which the MESSENGER mission was selected.

MESSENGER will be the first spacecraft to visit Mercury in more than 30 years and the first spacecraft to be placed in orbit about that planet. Observations to be made during the MESSENGER mission can be expected to advance substantially our knowledge of the formation and evolution of Mercury and of the terrestrial planets in general. Comparative studies of planetary geology, planetary composition and structure, magnetic field generation, and planetary exospheres and magnetospheres will all benefit from the new information that MESSENGER will reveal.

Acknowledgements

We thank Janice Dunlap, Sandra Keiser, and Barbara Northrop for assistance with manuscript preparation. The MESSENGER mission is supported by the NASA Discovery Program under contracts to the Carnegie Institution of Washington (NASW-00002) and The Johns Hopkins University Applied Physics Laboratory (NAS5-97271).

References

Acuña, M.H., Connerney, J.E.P., Wasilewski, P., Lin, R.P., Anderson, K.A., Carlson, C.W., McFadden, J., Curtis, D.W., Mitchell, D., Reme, H., Mazelle, C., Sanvand, J.A., d'Uston, C., Cros, A., Medale, J.L., Bauer, S.J., Cloutier, P., Mayhew, N., Winterhalter, D., Ness, N.F., 1998. Magnetic field and plasma observations at Mars: initial results of the Mars Global Surveyor mission. Science 279, 1676–1680.

Anderson, J.D., Jurgens, R.F., Lau, E.L., Slade III, M.A., Schubert, G., 1996. Shape and orientation of Mercury from radar ranging data. Icarus 124, 690–697.

Armstrong, T.P., Krimigis, S.M., Lanzerotti, L.J., 1975. A reinterpretation of the reported energetic particle fluxes in the vicinity of Mercury. J. Geophys. Res. 80, 4015–4017.

Baker, D.N., Simpson, J.A., Eraker, J.H., 1986. A model of impulsive acceleration and transport of energetic particles in Mercury's magnetosphere. J. Geophys. Res. 91, 8742–8748.

Barlow, N.G., Allen, R.A., Vilas, F., 1999. Mercurian impact craters: implications for polar ground ice. Icarus 141, 194–204.

Belton, M.J.S., Gierasch, P.J., Smith, M.D., Helfenstein, P., Schinder, P.J., Pollack, J.B., Rages, K.A., Ingersoll, A.P., Klaasen, K.P., Veverka, J., Anger, C.D., Carr, M.H., Chapman, C.R., Davies, M.E., Fanale, F.P., Greeley, R., Greenberg, R., Head III, J.W., Morrison, D., Neukum, G., Pilcher, C.B., 1991. Images from Galileo of the Venus cloud deck. Science 253, 1531–1536.

Benz, W., Slattery, W.L., Cameron, A.G.W., 1988. Collisional stripping of Mercury's mantle. Icarus 74, 516–528.

Bida, T.A., Killen, R.M., Morgan, T.H., 2000. Discovery of calcium in Mercury's atmosphere. Nature 404, 159–161.

Blewett, D.T., Lucey, P.G., Hawke, B.R., Ling, G.G., Robinson, M.S., 1997. A comparison of Mercurian reflectance and spectral quantities with those of the Moon. Icarus 129, 217–231.

Broadfoot, A.L., Kumar, S., Belton, M.J.S., McElroy, M.B., 1974. Mercury's atmosphere from Mariner 10: preliminary results. Science 185, 166–169.

Broadfoot, A.L., Shemansky, D.E., Kumar, S., 1976. Mariner 10: Mercury atmosphere. Geophys. Res. Lett. 3, 577–580.

Brückner, J., Masarik, J., 1997. Planetary gamma-ray spectroscopy of the surface of Mercury. Planet. Space Sci. 45, 39–48.

Butler, B.J., Muhleman, D.O., Slade, M.A., 1993. Mercury: full-disk radar images and the detection and stability of ice at the North Pole. J. Geophys. Res. 98, 15,003–15,023.

Cameron, A.G.W., 1985. The partial volatilization of Mercury. Icarus 64, 285–294.

Cassen, P., Young, R.E., Schubert, G., Reynolds, R.T., 1976. Implications of an internal dynamo for the thermal history of Mercury. Icarus 28, 501–508.

Chase, S.C., Miner, E.D., Morrison, D., Münch, G., Neugebauer, G., Schroeder, M., 1974. Preliminary infrared radiometry of the night side of Mercury from Mariner 10. Science 185, 142–145.

Cheng, A.F., Johnson, R.E., Krimigis, S.M., Lanzerotti, L.J., 1987. Magnetosphere, exosphere, and surface of Mercury. Icarus 71, 430–440.

Christon, S.P., Feynman, J., Slavin, J.A., 1987. Dynamic substorm injections: similar magnetospheric phenomena at Earth and Mercury. In: Lui, A.T.Y. (Ed.), Magnetotail Physics. Johns Hopkins University Press, Baltimore, MD, pp. 393–400.

Connerney, J.E.P., Ness, N.F., 1988. Mercury's magnetic field and interior. In: Vilas, F., Chapman, C.R., Matthews, M.S. (Eds.), Mercury. University of Arizona Press, Tucson, pp. 494–513.

Eraker, J.H., Simpson, J.A., 1986. Acceleration of charged particles in Mercury's manetosphere. J. Geophys. Res. 91, 9973–9993.

Esposito, L.W., 1984. Sulfur dioxide: episodic injection shows evidence for active Venus volcanism. Science 223, 1072–1074.

Evans, L.G., Squyres, S.W., 1987. Investigation of Martian H_2O and CO_2 via orbital gamma-ray spectroscopy. J. Geophys. Res. 92, 9153–9167.

Fegley Jr., B., Cameron, A.G.W., 1987. A vaporization model for iron/silicate fractionation in the Mercury protoplanet. Earth Planet. Sci. Lett. 82, 207–222.

Feldman, W.C., Barraclough, B.L., Hansen, C.J., Sprague, A.L., 1997. The neutron signature of Mercury's volatile polar deposits. J. Geophys. Res. 102, 25 565–25 574.

Fricker, P.E., Reynolds, R.T., Summers, A.L., Cassen, P.M., 1976. Does Mercury have a molten core? Nature 259, 293–294.

Gault, D.E., Guest, J.E., Murray, J.B., Dzurisin, D., Malin, M.C., 1975. Some comparisons of impact craters on Mercury and the Moon. J. Geophys. Res. 80, 2444–2460.

Goettel, K.A., Barshay, S.S., 1978. The chemical equilibrium model for condensation in the solar nebula: assumptions, implications and limitations. In: Dermott, S. (Ed.), The Origin of the Solar System. Wiley, Chichester, pp. 611–627.

Gold, R.E., Solomon, S.C., McNutt Jr., R.L., Santo, A.G., Abshire, J.B., Acuña, M.H., Afzal, R.S., Anderson, B.J., Andrews, G.B., Bedini, P.D., Cain, J., Cheng, A.F., Evans, L.G., Follas, R.B., Gloeckler, G., Goldsten, J.O., Hawkins III, S.E., Izenberg, N.R., Jaskulek, S.E., Ketchum, E.A., Lankton, M.R., Lohr, D.A., Mauk, B.H., McClintock, W., Murchie, S.L., Schlemm II, C.E., Smith, D.E., Starr, R.D., Zurbuchen, T.H., 2001. The MESSENGER mission to Mercury: scientific payload. Planet. Space Sci., this issue.

Goldstein, B.E., Suess, S.T., Walker, R.J., 1981. Mercury: magnetospheric processes and the atmospheric supply and loss rates. J. Geophys. Res. 86, 5485–5499.

Haines, E.L., Metzger, A.E., 1984a. Measuring planetary hydrogen by remote gamma-ray sensing. Nucl. Instrum. Methods Phys. Res. A 226, 509–516.

Haines, E.L., Metzger, A.E., 1984b. Measuring planetary neutron albedo fluxes by remote gamma-ray sensing. Nucl. Instrum. Methods Phys. Res. A 226, 517–523.

Hapke, B., Christman, C., Rava, B., Mosher, J., 1980. A color-ratio map of Mercury. Proceedings of the Lunar Scientific Conference 11th, pp. 817–821.

Harmon, J.K., 1997. Mercury radar studies and lunar comparisons. Adv. Space Res. 19, 1487–1496.

Harmon, J.K., Slade, M.A., 1992. Radar mapping of Mercury: full-disk images and polar anomalies. Science 258, 640–642.

Harmon, J.K., Slade, M.A., Velez, R.A., Crespo, A., Dryer, M.J., Johnson, J.M., 1994. Radar mapping of Mercury's polar anomalies. Nature 369, 213–215.

Hood, L.L., Schubert, G., 1979. Inhibition of solar wind impingement on Mercury by planetary induction currents. J. Geophys. Res. 84, 2641–2647.

Hunten, D.M., Morgan, T.H., Shemansky, D.E., 1988. The Mercury atmosphere. In: Vilas, F., Chapman, C.R., Matthews, M.S. (Eds.), Mercury. University of Arizona Press, Tucson, pp. 562–612.

Ingersoll, A.P., Svitek, T., Murray, B.C., 1992. Stability of polar frosts in spherical bowl-shaped craters on the Moon, Mercury, and Mars. Icarus 100, 40–47.

Jeanloz, R., Mitchell, D.L., Sprague, A.L., de Pater, I., 1995. Evidence for a basalt-free surface on Mercury and implications for internal heat. Science 268, 1455–1457.

Killen, R.M., Potter, A.E., Morgan, T.H., 1990. The spatial distribution of sodium in Mercury's exosphere. Icarus 85, 145–167.

Killen, R.M., Benkoff, J., Morgan, T.H., 1997. Mercury's polar caps and the generation of an OH exosphere. Icarus 125, 195–211.

Kivelson, M.G., Khurana, K.K., Russell, C.T., Walker, R.J., Warnecke, J., Coroniti, F.V., Polanskey, C., Southwood, D.J., Schubert, G., 1996. Discovery of Ganymede's magnetic field by the Galileo spacecraft. Nature 384, 537–541.

Kliore, A.J., Cain, D.L., Fjeldbo, G., Seidel, B.L., Sykes, M.J., 1972. The atmosphere of Mars from Mariner 9 radio occultation measurements. Icarus 17, 484–516.

Lebach, D.E., Corey, B.E., Shapiro, I.I., Ratner, M.I., Webber, J.C., Rogers, A.E.E., Davis, J.L., Herring, T.A., 1995. Measurement of the

solar gravitational deflection of radio waves using very-long-baseline interferometry. Phys. Rev. Lett. 75, 1439–1442.
Lewis, J.S., 1972. Metal/silicate fractionation in the solar system. Earth Planet. Sci. Lett. 15, 286–290.
Lewis, J.S., 1988. Origin and composition of Mercury. In: Vilas, F., Chapman, C.R., Matthews, M.S. (Eds.), Mercury. University of Arizona Press, Tucson, pp. 651–669.
Lindal, G.F., Hotz, H.B., Sweetnam, D.N., Shippony, Z., Brenkle, J.P., Hartsell, G.V., Spear, R.T., Michael Jr., W.H., 1979. Viking radio occultation measurements of the atmosphere and topography of Mars: data acquired during 1 Martian year of tracking. J. Geophys. Res. 84, 8443–8456.
Lisse, C.M., Dennerl, K., Englhauser, J., Harden, M., Marshall, F.E., Mumma, M.J., Petre, R., Pye, J.P., Ricketts, M.J., Schmitt, J., Trümper, J., West, R.G., 1996. Discovery of X-ray and extreme ultraviolet emission from Comet C/Hyakutake 1996 B2. Science 274, 205–209.
Luhmann, J.G., Russell, C.T., Tsyganenko, N.A., 1998. Disturbances in Mercury's magnetosphere: are the Mariner 10 "substorms" simply driven? J. Geophys. Res. 103, 9113–9119.
McGrath, M.A., Johnson, R.E., Lanzerotti, L.J., 1986. Sputtering of sodium on the planet Mercury. Nature 323, 694–696.
Melosh, H.J., Dzurisin, D., 1978. Mercurian global tectonics: a consequence of tidal despinning? Icarus 35, 227–236.
Melosh, H.J., McKinnon, W.B., 1988. The tectonics of Mercury. In: Vilas, F., Chapman, C.R., Matthews, M.S. (Eds.), Mercury. University of Arizona Press, Tucson, pp. 374–400.
Morgan, T.H., Killen, R.M., 1997. A non-stoichiometric model of the composition of the atmospheres of Mercury and the Moon. Planet. Space Sci. 45, 81–94.
Moses, J.I., Rawlins, K., Zahnle, K., Downs, L., 1999. External sources of water for Mercury's putative ice deposits. Icarus 137, 197–221.
Murray, B.C., 1975. The Mariner 10 pictures of Mercury: an overview. J. Geophys. Res. 80, 2342–2344.
Ness, N.F., Behannon, K.W., Lepping, R.P., Whang, Y.C., Schatten, K.H., 1974. Magnetic field observations near Mercury: preliminary results from Mariner 10. Science 185, 151–160.
Ness, N.F., Behannon, K.W., Lepping, R.P., Whang, Y.C., 1975. The magnetic field of Mercury, 1. J. Geophys. Res. 80, 2708–2716.
Ness, N.F., Behannon, K.W., Lepping, R.P., Whang, Y.C., 1976. Observations of Mercury's magnetic field. Icarus 28, 479–488.
Ogilvie, K.W., Scudder, J.D., Hartle, R.E., Siscoe, G.L., Bridge, H.S., Lazarus, A.J., Asbridge, J.R., Bame, S.J., Yeates, C.M., 1974. Observations at Mercury encounter by the plasma science experiment on Mariner 10. Science 185, 145–151.
Paige, D.A., Wood, S.E., Vasavada, A.R., 1992. The thermal stability of water ice at the poles of Mercury. Science 258, 643–646.
Peale, S.J., 1972. Determination of parameters related to the interior of Mercury. Icarus 17, 168–173.
Peale, S.J., 1976. Does Mercury have a molten core? Nature 262, 765–766.
Peale, S.J., 1981. Measurement accuracies required for the determination of a Mercurian liquid core. Icarus 48, 143–145.
Peale, S.J., 1988. The rotational dynamics of Mercury and the state of its core. In: Vilas, F., Chapman, C.R., Matthews, M.S. (Eds.), Mercury. University of Arizona Press, Tucson, pp. 461–493.
Peale, S.J., 1997. Characterizing the core of Mercury. Lunar Planet. Sci. 28, 1081–1082.
Phillips, R.J., Solomon, S.C., 1997. Compressional strain history of Mercury. Lunar Planet. Sci. 28, 1107–1108.
Potter, A.E., Morgan, T.H., 1985. Discovery of sodium in the atmosphere of Mercury. Science 229, 651–653.
Potter, A.E., Morgan, T.H., 1986. Potassium in the atmosphere of Mercury. Icarus 67, 336–340.
Rava, B., Hapke, B., 1987. An analysis of the Mariner 10 color ratio map of Mercury. Icarus 71, 397–429.
Reasenberg, R.D., Shapiro, I.I., MacNeil, P.E., Goldstein, R.B., Breidenthal, J.C., Brenkle, J.P., Cain, D.L., Kaufman, T.M., Komarek, T.A., Zygielbaum, A.I., 1979. Viking relativity experiment: verification of signal retardation by solar gravity. Astrophys. J. 234, L219–L221.
Robinson, M.S., Lucey, P.G., 1997. Recalibrated Mariner 10 color mosaics: implications for Mercurian volcanism. Science 275, 197–200.
Robinson, M.S., Davies, M.E., Colvin, T.R., Edwards, K., 1999. A revised control network for Mercury. J. Geophys. Res. 104, 30,847–30,852.
Russell, C.T., Baker, D.N., Slavin, J.A., 1988. The magnetosphere of Mercury. In: Vilas, F., Chapman, C.R., Matthews, M.S. (Eds.), Mercury. University of Arizona Press, Tucson, pp. 514–561.
Santo, A.G., Gold, R.E., McNutt Jr., R.L., Solomon, S.C., Ercol, C.J., Farquhar, R.W., Hartka, T.J., Jenkins, J.E., McAdams, J.V., Mosher, L.E., Persons, D.F., Artis, D.A., Bokulic, R.S., Conde, R.F., Dakermanji, G., Goss Jr., M.E., Haley, D.R., Heeres, K.J., Maurer, R.H., Moore, R.C., Rodberg, E.H., Stern, T.G., Wiley, S.R., Williams, B.G., Yen, C.L., Peterson, M.R., 2001. The MESSENGER mission to Mercury: spacecraft and mission design. Planet. Space Sci., this issue.
Schubert, G., Ross, M.N., Stevenson, D.J., Spohn, T., 1988. Mercury's thermal history and the generation of its magnetic field. In: Vilas, F., Chapman, C.R., Matthews, M.S. (Eds.), Mercury. University of Arizona Press, Tucson, pp. 429–460.
Schubert, G., Zhang, K., Kivelson, M.G., Anderson, J.D., 1996. The magnetic field and internal structure of Ganymede. Nature 384, 544–545.
Shapiro, I.I., Pettengill, G.H., Ash, M.E., Ingalls, R.P., Campbell, D.B., Dyce, R.B., 1972. Mercury's perihelion advance: determination by radar. Phys. Rev. Lett. 28, 1594–1597.
Siegfried, R.W., Solomon, S.C., 1974. Mercury: internal structure and thermal evolution. Icarus 23, 192–205.
Simons, M., Solomon, S.C., Hager, B.H., 1997. Localization of gravity and topography: constraints on the tectonics and mantle dynamics of Venus. Geophys. J. Int. 131, 24–44.
Simpson, J.A., Eraker, J.H., Lamport, J.E., Walpole, P.H., 1974. Electrons and protons accelerated in Mercury's magnetic field. Science 185, 160–166.
Siscoe, G.L., Christopher, L., 1975. Variations in the solar wind stand-off distance at Mercury. Geophys. Res. Lett. 2, 158–160.
Siscoe, G.L., Ness, N.F., Yeates, C.M., 1975. Substorms on Mercury? J. Geophys. Res. 80, 4359–4363.
Slade, M.A., Butler, B.J., Muhleman, D.O., 1992. Mercury radar imaging: evidence for polar ice. Science 258, 635–640.
Slavin, J.A., Holzer, R.E., 1979a. The effect of erosion on the solar wind stand-off distance at Mercury. J. Geophys. Res. 84, 2076–2082.
Slavin, J.A., Holzer, R.E., 1979b. On the determination of the Hermean magnetic moment: a critical review. Phys. Earth Planet. Inter. 20, 231–236.
Slavin, J.A., Owen, C.J., Connerney, J.E.P., Christon, S.P., 1997. Mariner 10 observations of field-aligned currents at Mercury. Planet. Space Sci. 45, 133–141.
Smith, D.E., Zuber, M.T., 1996. The shape of Mars and the topographic signature of the hemispheric dichotomy. Science 271, 184–188.
Smythe, W.H., Marconi, M.L., 1995. Theoretical overview and modeling of the sodium and potassium atmospheres of Mercury. Astrophys. J. 441, 839–864.
Solomon, S.C., 1976. Some aspects of core formation in Mercury. Icarus 28, 509–521.
Solomon, S.C., Head, J.W., 1990. Heterogeneities in the thickness of the elastic lithosphere of Mars: constraints on heat flow and internal dynamics. J. Geophys. Res. 95, 11,073–11,083.
Solomon, S.C., Comer, R.P., Head, J.W., 1982. The evolution of impact basins: viscous relaxation of topographic relief. J. Geophys. Res. 87, 3975–3992.
Sprague, A.L., 1990. A diffusion source for sodium and potassium in the atmospheres of Mercury and the Moon. Icarus 84, 93–105.
Sprague, A.L., Kozlowski, R.W.H., Witteborn, F.C., Cruikshank, D.P., Wooden, D.H., 1994. Mercury: evidence for anorthosite and basalt from mid-infrared (7.5–13.5μm) spectroscopy. Icarus 109, 156–167.
Sprague, A.L., Hunten, D.M., Lodders, K., 1995. Sulfur at Mercury, elemental at the poles and sulfides in the regolith. Icarus 118, 211–215.

Sprague, A.L., Hunten, D.M., Grosse, F.A., 1996. Upper limit for lithium in Mercury's atmosphere. Icarus 123, 345–349.

Sprague, A.L., Nash, D.B., Witteborn, F.C., Cruikshank, D.P., 1997. Mercury's feldspar connection mid-IR measurements suggest plagioclase. Adv. Space Res. 19, 1507–1510.

Spudis, P.D., Guest, J.E., 1988. Stratigraphy and geologic history of Mercury. In: Vilas, F., Chapman, C.R., Matthews, M.S. (Eds.), Mercury. University of Arizona Press, Tucson, pp. 118–164.

Spudis, P.D., Prosser, J.G., 1984. Geologic map of the Michelangelo quadrangle of Mercury. Map I-1659, United States Geological Survey, Washington, DC.

Srnka, L.J., 1976. Magnetic dipole moment of a spherical shell with TRM acquired in a field of internal origin. Phys. Earth Planet. Inter. 11, 184–190.

Stephenson, A., 1976. Crustal remanence and the magnetic moment of Mercury. Earth Planet. Sci. Lett. 28, 454–458.

Stevenson, D.J., 1987. Mercury's magnetic field: a thermoelectric dynamo? Earth Planet. Sci. Lett. 82, 114–120.

Strom, R.G., 1979. Mercury: a post-Mariner 10 assessment. Space. Sci. Rev. 24, 3–70.

Strom, R.G., 1997. Mercury: an overview. Adv. Space Res. 19, 1471–1485.

Strom, R.G., Trask, N.J., Guest, J.E., 1975. Tectonism and volcanism on Mercury. J. Geophys. Res. 80, 2478–2507.

Trombka, J.I., Floyd, S.R., Boynton, W.V., Bailey, S., Brückner, J., Squyres, S.W., Evans, L.G., Clark, P.E., Starr, R., Fiore, E., Gold, R., Goldsten, J., McNutt, R., 1997. The NEAR X-ray/gamma-ray spectrometer. J. Geophys. Res. 102, 23,729–23,750.

Vilas, F., 1988. Surface composition of Mercury from reflectance spectrophotometry. In: Vilas, F., Chapman, C.R., Matthews, M.S. (Eds.), Mercury. University of Arizona Press, Tucson, pp. 59–76.

Vilas, F., Chapman, C.R., Matthews, M.S. (Eds.), 1988. Mercury. University of Arizona Press, Tucson, 794 pp.

Watters, T.R., Robinson, M.S., Cook, A.C., 1998. Topography of lobate scraps on Mercury: new constraints on the planet's contraction. Geology 26, 991–994.

Weidenschilling, S.J., 1978. Iron/silicate fractionation and the origin of Mercury. Icarus 35, 99–111.

Wetherill, G.W., 1988. Accumulation of Mercury from planetesimals. In: Vilas, F., Chapman, C.R., Matthews, M.S. (Eds.), Mercury. University of Arizona Press, Tucson, pp. 670–691.

Wetherill, G.W., 1994. Provenance of the terrestrial planets. Geochim. Cosmochim. Acta 58, 4513–4520.

Williams, D.J., McEntire, R.W., Krimigis, S.M., Roelef, E.C., Jaskulek, S., Tossman, B.E., Wilken, B., Stüdemann, W., Armstrong, T.P., Fritz, T.A., Lanzerotti, L.J., Roederer, J.G., 1991. Energetic particles at Venus: Galileo results. Science 253, 1525–1528.

Wu, X., Bender, P.L., Rosborough, G.W., 1995. Probing the interior structure of Mercury from an orbiter plus single lander. J. Geophys. Res. 100, 1515–1525.

Wu, X., Bender, P.L., Peale, S.J., Rosborough, G.W., Vincent, M.A., 1997. Determination of Mercury's 88-day libration and fluid core size from orbit. Planet. Space Sci. 45, 15–19.

Zuber, M.T., Smith, D.E., 1997. Remote sensing of planetary librations from gravity and topography data: Mercury simulation. Lunar Planet. Sci. 28, 1637–1638.

Zuber, M.T., Smith, D.E., Lemoine, F.G., Neumann, G.A., 1994. The shape and internal structure of the Moon from the Clementine mission. Science 266, 1839–1843.